FSE FONDO SOCIALE EUROPEO
SICILIA 2020
PROGRAMMA OPERATIVO

Ph.D. in Physics, XXXVI cycle (FIS/03)

Università degli studi di Messina

Dipartimento di Scienze Matematiche e Informatiche, Scienze Fisiche

e Scienze della Terra

Fabio Mauceri

HYBRID QUANTUM SYSTEMS IN THE USC REGIME

Tutor:

Prof. O. Di Stefano

Ph.D. Coordinator:

Prof. V. Crupi

CoTutor:

Prof. S. Savasta

Academic year 2022/2023

Abstract

The interaction between light and matter is one of the most fundamental phenomena in physics, and it has been extensively studied in various contexts, such as atomic physics, quantum optics, and solid-state physics. In particular, the regime of strong coupling, where the light-matter interaction energy exceeds the dissipation rates of the system, has attracted a lot of attention for its potential applications in quantum information processing, quantum metrology, and quantum simulation. However, in recent years, new regimes of light-matter interaction have emerged, where the coupling strength becomes comparable to or even larger than the bare frequencies of the subsystems. These regimes, known as the ultrastrong coupling regime and the deep-strong coupling regime, pose new challenges and opportunities for both theoretical and experimental investigations. In particular, it has been shown that as the coupling enters the ultrastrong coupling regime, many issues arise, like the violation of the gauge invariance principle, and the presence of virtual excitations in the ground state.

In this thesis, I explore some novel aspects of the ultrastrong coupling (USC) and deep-strong coupling (DSC) regimes on hybrid systems. The focus will be on cavity quantum electrodynamics and I will use two prototypical models: the quantum Rabi model and the Hopfield model, which describe the interaction between a single-mode cavity field and a two-level system, or a multimode cavity field and a collection of two-level systems, respectively. I also consider the effects of pure dephasing, which originates from the non-dissipative information exchange between quantum systems and environments, and plays a key role in both spectroscopy and quantum information technology. Additionally, I will study the hopping mechanism in optomechanics.

The main results of this thesis are as follows:

- I derive an effective Hamiltonian for a nonlinear oscillator coupled to a qubit

using a polariton model. I show the importance of correctly applying the minimal coupling to satisfy the gauge invariance principle.

- I investigate the pure dephasing of light-matter systems in the USC and DSC regimes, using a dissipative quantum Rabi model and a Hopfield model. I find that the interaction can significantly affect the form of the stochastic perturbation describing the dephasing of a subsystem, depending on the adopted gauge.

- I study the optomechanical two-photon hopping in a system of two cavities separated by a vibrating two-sided perfect mirror. I show that this system displays photon-pair hopping between the two electromagnetic resonators, which is not due to tunnelling, but rather to higher-order resonant processes.

This thesis is organized as follows:

- In Chapter 1, I introduce the basic concepts and tools of cavity quantum electrodynamics and the USC and DSC regimes.

- In Chapter 2, I present the model and the results for the nonlinear oscillator both uncoupled and coupled to a qubit.

- In Chapter 3, I present the model and the results for the pure dephasing of light-matter systems.

- In Chapter 4, I present the model and the results for the optomechanical two-photon hopping.

- In Chapter 5, I summarize the main conclusions and outlooks of this thesis.

List of publications

- F. Mauceri, A. Mercurio, S. Savasta and O. Di Stefano, "Ultrastrong coupling of a qubit with a nonlinear optical resonator", *Physical Review A* (2022), 105(2), 023719.
- A. Mercurio, S. Abo, F. Mauceri, E. Russo, V. Macrì, A. Miranowicz, S. Savasta and O. Di Stefano, "Pure Dephasing of Light-Matter Systems in the Ultrastrong and Deep-Strong Coupling Regimes", *Physical Review Letters* (2023), 130(12), 123601.
- E. Russo, A. Mercurio, F. Mauceri, R. Lo Franco, F. Nori, S. Savasta and V. Macrì, "Optomechanical two-photon hopping", *Physical Review Research* (2023), 5(1), 013221.

Fundings

This Ph.D was funded by Regione Siciliana, Fondo Sociale Europeo (FSE) and partially by Army Research Office (ARO) (Grant No. W911NF1910065).

Contents

List of Tables

List of Figures

List of Abbreviations and Symbols

Abbreviations

WC	weak coupling
SC	strong coupling
USC	ultrastrong coupling
DSC	deep-strong coupling
cQED	cavity quantum electrodynamics
QDs	single quantum dots
QIP	quantum information processing
η	normalized coupling strength
κ	atomic losses
γ	photonic losses
JCM	Jaymes-Cumming model
QRM	quantum Rabi model
ME	master equation
RWA	rotating wave approximation

Chapter 1

Introduction: Light-matter coupling

With light-matter interaction we usually intend processes that involve the absorption, emission or scattering of a photon by a distribution of charges. This definition follows a perturbative description of quantum electrodynamics, where the strength of the interactions is related to the dimensionless fine structure constant $\alpha \simeq \frac{1}{137}$. The smallness of α explains why a satisfactory description is obtained by considering only first (absorption and emission) or second (scattering) order processes.

In 1946 Purcell [1] showed that, while the value of α is fixed by nature, it was possible to engineer systems with a modified coupling strength, usually indicated with the letter g. In these systems is possible to increase or decrease the lifetime of an excited state by modifying the local density of photonic states at the emitter position. For example, Chang et al. [2] were able to experimentally demonstrate full control of the spontaneous-emission dynamics of single quantum dots (QDs) in a photonic-crystal nanocavity, by showing time-resolved micro-photoluminescence intensities of InGaAs QDs on resonance with the cavity, off-resonance and in bulk without any cavity. Compared with the case without any cavity, the QDs decay more quickly in a resonant cavity (which enhances the density of states that the QDs can decay to) and more slowly in an off-resonant cavity (which shields the QDs from the environment).

This marked the birth of a new field of research called cavity quantum electrodynamics (cQED). A few decades later, this led to the possibility of building devices with low energy losses and controllable coupling strength. A cornerstone of this field is the Nobel

prize winner experiment by Haroche and co-workers [3], which in 1983 used a collection of Rydberg atoms in a high-Q microwave cavity to obtain a system whose coupling strength was bigger than its losses. This regime of coupling, known as the strong coupling (SC) regime, is characterized by coherent quantum dynamics and processes, like the quantum Rabi oscillation, where an excitation jumps back and forth between the cavity and an atom.

Now we can formally define the first scale of light-matter interaction. Comparing the coupling strength g with the photonic losses (γ) or atomic losses (κ), we say that the system is in the strong coupling regime when γ,$\kappa \geq g$ and in the weak coupling (WC) regime in other cases.

The ability to control the property of light-matter interaction with the Purcell effect in the WC regime, led to a plethora of applications and innovations such as low-threshold solid-state lasers [4] and efficient single-photon and entangled-photon emitters [5, 6], while the more experimentally complex SC regime made it possible to manipulate and control quantum systems, enabling tests of fundamental physics [7] and applications [8] such as high-precision measurements [9] and quantum information processing (QIP) [10].

A different scale is obtained by comparing g with the bare frequencies of the subsystems ω (with bare we intend the frequency of the non-interacting components of the system). Usually is considered that when the ratio between g and ω, called normalized coupling strength (η), is at least 0.1, the system is in the ultrastrong coupling (USC) regime, although this value should not be considered a hard threshold. Again, it is important to stress that the USC is not the SC with a stronger coupling, but they are two different scales. On the other hand, if we further increase the coupling in the USC regime, we enter another domain of interaction, called the deep-strong coupling (DSC). Both USC and DSC are characterized by the impossibility of separating light and matter states as they mix and, their properties get intertwined, as it will be explained in more detail later.

The achievement of these regimes is more recent, as the USC was first theoretically defined in 2005 by Ciuti et al. [11] and its first experimental observation in 2009 by Anappara et al. [12] by using intersubbands polaritons. Afterwards, greater coupling strength values were achieved in this kind of system, for example [13, 14], and many

other systems were brought into the USC regime: superconducting systems [15, 16, 17], Landau polaritons [18, 19, 20], organic molecules [21, 22, 23] and optomechanics [24, 25]. These are only some examples of a very extensive (and growing) literature, proving the vast interest in this topic, further stressed by two recent reviews [26, 27].

We are just starting to see the innovations that these interaction regimes can bring, but as with many other novelty, these new light-matter interaction regimes brought many questions, some of them still awaiting answers. Two of the big issues raised by the USC and DSC regimes are the so-called vacuum emission and the gauge dependence of the theoretical description [28]. Now these original questions are, for the most part, answered. Almost two decades after its introduction, we finally have a satisfying theoretical description and the technical skills that allow the fabrication of devices in these regimes.

Undoubtedly, in the coming years, we will witness the advent of more efficient devices that exploit USC and DSC regimes. For instance, the interaction between a single photon and a single emitter leads to significant nonlinearity, which has found applications in electro-optical devices operating in the SC regime. By transitioning from SC to USC, the performance of such devices will improve considerably. This transition enables faster control and response, even for components with shorter lifetimes. Moreover, certain quantum effects, including quantum gates in specific short-lifetime systems, can only be observed above the USC threshold. The list of emerging applications of USC is extensive and encompasses Quantum Information Processing (QIP), Quantum Metrology, Nonlinear Optics, Quantum Optomechanics, Quantum Plasmonics, Superconductivity, Metamaterials, Quantum Simulations, Quantum Thermodynamics, Chemistry QED, Materials Science, and more. Furthermore, it remains an open question whether entirely new phenomena can be predicted and observed within the USC or DSC regimes. For instance, experimental observations have revealed new stable states of matter. These states could be entangled hybrid light-matter ground states in the DSC regime [16] or as discrete time crystals, predicted [29] to exist in systems described by the Dicke model with tunable USC.

1.1 Quantum Rabi model

A single atom in a single frequency cavity is the simplest case of cavity QED and is described by the quantum Rabi model (QRM) [30, 31, 32]. This model considers the atom as a two-level system whose upper level $|e\rangle$ is connected to the lower level $|g\rangle$ by an electric dipole transition at angular frequency ω_q. This system is equivalent to a $\frac{1}{2}$ spin particle in an external magnetic field (conventionally oriented along the Z-axis) because the spin can only be parallel or antiparallel to the field, i.e. it has two energy levels and energy eigenstates. We make the correspondence $|e\rangle \to |0\rangle$ and $|g\rangle \to |1\rangle$, so that $|e\rangle$ and $|g\rangle$ are eigenstates of σ_z with eigenvalue $+1$ and -1. With these definitions, the atomic Hamiltonian is ($\hbar = 1$):

$$\hat{\mathcal{H}}_q = \frac{\omega_q}{2}\hat{\sigma}_z\,. \tag{1.1.1}$$

Note that the state $|1\rangle$ has lower energy than the state $|0\rangle$. This is only a convention, so using the opposite definition is possible if convenient.

We also introduce the atomic raising and lowering operators $\sigma_\pm$:

$$\hat{\sigma}_\pm = \frac{1}{2}\left(\hat{\sigma}_x \pm i\hat{\sigma}_y\right)\,, \tag{1.1.2}$$

these atomic excitations creation and annihilation operators follow the fermionic commutation relation $[\hat{\sigma}_-, \hat{\sigma}_+] = 1$.

The single-frequency cavity (ω_c) is described with a bosonic harmonic resonator whose Hamiltonian is:

$$\hat{\mathcal{H}}_c = \omega_c \hat{a}^\dagger \hat{a}. \tag{1.1.3}$$

The classical coupling Hamiltonian is $-\boldsymbol{D}\cdot\boldsymbol{E}_c$, where $\boldsymbol{E}_c$ is the electric field and $\boldsymbol{D} = q\boldsymbol{R}$ is atomic dipole vector and $\boldsymbol{R}$. Assuming that $|0\rangle$ and $|1\rangle$ are levels of opposite parities, the odd-parity $q\hat{R}$ dipole operator is purely non-diagonal in the Hilbert space spanned by $|0\rangle$ and $|1\rangle$ and develops along the $\hat{\sigma}_\pm$ matrices according to:

$$\boldsymbol{D} = d\left(\boldsymbol{\epsilon}_a\hat{\sigma}_- + \boldsymbol{\epsilon}_a^*\hat{\sigma}_+\right), \tag{1.1.4}$$

where we have introduced the notation:

$$q\left\langle g\right|\hat{R}\left|e\right\rangle = d\boldsymbol{\epsilon}_a, \tag{1.1.5}$$

with d being the dipole matrix element of the atomic transition and $\boldsymbol{\epsilon}_a$ the polarization vector. The electric field is:

$$\mathbf{E}_r = i\mathcal{E}_r\left[\boldsymbol{\epsilon}_r e^{-i\omega_r t}e^{-i\varphi} - \boldsymbol{\epsilon}_r^* e^{+i\omega_r t}e^{i\varphi}\right]\,, \tag{1.1.6}$$

where $\mathcal{E}_r$ is the real amplitude of the classical field, ω_r is its frequency, $\boldsymbol{\epsilon}_r$ is the complex unit vector describing its polarization and φ is its phase. Following the usual quantization procedure, we obtain the interaction Hamiltonian $\hat{\mathcal{H}}_{\text{int}} = \eta\omega_c \left(\hat{a}^\dagger + \hat{a}\right)(\hat{\sigma}_+ + \hat{\sigma}_-)$, so the quantum Rabi Hamiltonian in the dipole gauge is:

$$\hat{\mathcal{H}}_d = \omega_c \hat{a}^\dagger \hat{a} + \frac{\omega_q}{2}\hat{\sigma}_z + \eta\omega_c \left(\hat{a}^\dagger + \hat{a}\right)(\hat{\sigma}_+ + \hat{\sigma}_-) \ . \tag{1.1.7}$$

The interaction Hamiltonian consists of four terms, two of them $\left(\hat{a}^\dagger\hat{\sigma}_- + \hat{a}\hat{\sigma}_+\right)$ called rotating or co-rotating terms and the other two $\left(\hat{a}^\dagger\hat{\sigma}_+ + \hat{a}\hat{\sigma}_-\right)$ called counter-rotating or anti-resonant terms. The rotating terms conserve the number of excitations since they create one excitation in one field and destroy one in the other, while the counter-rotating terms create or destroy two simultaneously in both fields.

Outside of the USC and DSC regimes, i.e. for coupling $\eta \lesssim 0.1$, is possible to apply the rotating wave approximation (RWA) and discard the counter-rotating terms, obtaining the well-known Jaymes-Cumming model (JCM) [32]. The eigenstates of the JCM are also called 'dressed states' and, due to the exclusive presence of exchange terms in the Hamiltonian of the JCM, only states with an equal number of excitations are capable of interacting. For each excitation is possible to identify two states $|+\rangle$ and $|-\rangle$, called JC doublets. They are superpositions of two states containing both light and matter excitations. Considering this, a full diagonalization can be obtained in a subspace of n JC doublets $|\pm\rangle_n$, with n number of excitations. This model has had widespread use in a variety of physical platforms, ranging from neutral atoms in optical and microwave cavities, trapped ions with quantized motion, to superconducting qubits coupled to electromagnetic cavities, transmission line resonators, and nanomechanical resonators.

By contrast, lifting the RWA and considering the full Rabi Hamiltonian has intrinsic difficulties but the most relevant are the presence of virtual excitations in the ground state [33, 34] and the violation of the gauge principle [28, 35].

1.1.1 Virtual excitations in the ground state

Before addressing the problem of the virtual excitations in the ground state, it is interesting to talk about the eigenstates of the QRM. As the coupling strength increases and the counter-rotating terms can be no longer neglected, the number of excitations ($\hat{N}_{\text{exc}} = \hat{a}^\dagger\hat{a} + \hat{\sigma}_+\hat{\sigma}_-$) is no longer conserved and states with different numbers of excita-

tions can interact and get hybridised, leading to the phenomenology that distinguishes USC with non-USC regimes. The dressing of the eigenvalue is no longer restricted to two levels at a time, defined by a fixed number of excitations, but multiple bare levels with different numbers of excitations participate in the dressing process. This posed a challenging problem and the QRM was long considered to be unsolvable by analytical means and also non-integrable [36], until an analytic solution was found in 2011 by Braak [37], although it still requires the numerical calculation of transcendental functions.

Indeed, the Rabi Hamiltonian presented in (1.1.7) has a conserved quantity, the parity operator $\hat{P} = \exp\left(i\pi\hat{N}_{\text{exc}}\right)$, but, is also possible to generalize this model, a necessity in superconducting circuits [15, 16], breaking even the parity symmetry [38]. This model is called asymmetrical QRM and is obtained by replacing the interaction term $\left(\hat{a}^\dagger + \hat{a}\right)(\hat{\sigma}_+ + \hat{\sigma}_-) = \left(\hat{a}^\dagger + \hat{a}\right)\hat{\sigma}_x$ with $\left(\hat{a}^\dagger + \hat{a}\right)(\cos\theta\hat{\sigma}_x + \sin\theta\hat{\sigma}_z)$, considering $\theta \neq 0, \pi$.

The presence of excitations in the ground state is maybe *the* distinguishing property between USC and non-USC regimes. As shown in see Fig. 1.1 (from [26]), as the coupling strength increases the mean value in the ground state of both $\left\langle \hat{a}^\dagger\hat{a} \right\rangle$ and $\langle \hat{\sigma}_-\hat{\sigma}_+ \rangle$ increases. One of the first points discussed at the birth of USC was the nature of these excitations. Since the mean value $\left\langle \hat{a}^\dagger\hat{a} \right\rangle_{\text{gs}} \neq 0$ does it mean that in USC even the ground state will radiate? If it does not and the excitations are only virtual, how can they enable non-linear processes like the one shown by Kockum et al. [39]?

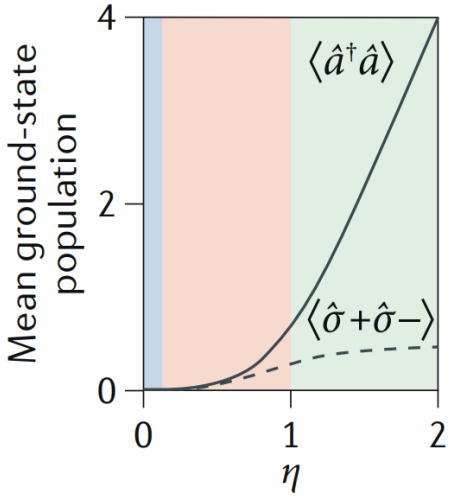

Figure 1.1: Mean number of virtual photonic and atomic excitation in the ground state. As the coupling increases, the ground state of the quantum QRM starts to contain a considerable number of (virtual) atomic and photonic excitations

A first solution considering the colored nature of the dissipation bath was proposed by Ciuti et al. [33], but this method is numerically demanding. A different, less computationally onerous solution was proposed by Ridolfo et al. [34]. Both paths show that the excitations contained in USC states are indeed *virtual*, "trapped" in the states and unable to be emitted. Following the approach by Ridolfo et al. [34], let us recall Glauber's photodetection theory [40]. He defined $\hat{E}^-$ and $\hat{E}^+$ as the positive and negative frequency components of the electric field operator of the output field to be used in photodetection. The probability per unit time that a photon be absorbed by an ideal detector is proportional to $\left\langle \hat{E}^-(t)\hat{E}^+(t)\right\rangle$. This quantity calculated in the ground state must be zero, otherwise it would not be a ground state, since if it emits then it is decaying into a lower energy state, defying the definition of ground state. With this in mind, the only explanation is that $\hat{a}^\dagger$ and $\hat{a}$ are not the correct operators to use in photodetection. This becomes evident when we consider the electric field operator in the dressed basis, i.e. $\langle j|\,\hat{a}+\hat{a}^\dagger\,|k\rangle$. For coupling strength close to zero, $\langle j|\,\hat{a}\,|k\rangle$ generate the positive frequency component of the electric field operator, while $\langle j|\,\hat{a}^\dagger\,|k\rangle$ generates the negative frequency components. But, as the coupling strength increases and we enter the USC regime, that is not the case, as both $\langle j|\,\hat{a}\,|k\rangle$ and $\langle j|\,\hat{a}^\dagger\,|k\rangle$ are not exclusively composed by positive or negative frequency. On the other hand, considering $\langle j|\,\hat{a}+\hat{a}^\dagger\,|k\rangle$ and defining its positive frequency component as $\hat{E}^-$ and its negative component as $\hat{E}^+$, ensures a consistent result.

Still, there needs to be a relation between the intra-cavity field $\hat{X}^-$ and $\hat{X}^+$ and the extra-cavity $\hat{a}$ and $\hat{a}^\dagger$, and to derive it we consider a cavity coupled to an output waveguide via the standard position-momentum interaction, i.e. an interaction between the cavity field $\hat{X}$ and the momentum quadrature $\hat{\Pi}_\omega$ of the waveguide field outside the cavity. Therefore the interaction Hamiltonian is $\hat{H}_{\rm i} = \epsilon_c \int d\omega \hat{X}\hat{\Pi}_\omega$, with $\hat{\Pi}_\omega = -i\sqrt{\omega/4\pi\epsilon_0\nu}\left[\hat{a}_\omega - \hat{a}_\omega^\dagger\right]$, where ϵ_c is a coupling parameter, ϵ_0 is a parameter describing the dielectric properties of the output waveguide and ν is the phase velocity.

The input (output) field operators are:

$$\hat{a}_{\rm out(in)}(t) = \frac{1}{\sqrt{2\pi}}\int d\omega\sqrt{\omega}e^{-i\omega(t-\bar{t})}\hat{a}_\omega(\tilde{t}), \tag{1.1.8}$$

where $\tilde{t} = t_1 \to \infty$ for the input field and $\tilde{t} = t_0 \to -\infty$ for the output field. With this definition $\left\langle \hat{a}^\dagger_{\rm out}(t)\hat{a}_{\rm in}(t)\right\rangle$ is proportional to $\left\langle \hat{E}^-(t)\hat{E}^+(t)\right\rangle$, that describe the photon flux emitted by the cavity. Following the standard procedure [41], we obtain the input-output

relation:

$$\hat{a}_{\text{out}}(t) = \hat{a}_{\text{in}}(t) - i\frac{\epsilon_c}{\sqrt{8\pi^2\epsilon_o v}}\dot{\hat{X}}^+. \tag{1.1.9}$$

To separate $\hat{X}$ into its positive and negative frequency components $\dot{\hat{X}}^+$and $\dot{\hat{X}}^-$, we expand it in terms of the energy eigenstates $|j\rangle$ and find $\dot{\hat{X}}^+ = -i\sum_{j,k>j}\Delta_{kj}X_{jk}|j\rangle\langle k|$, where $X_{jk} = \langle j|\hat{X}|k\rangle$ and $\hat{X}^- = \left(\hat{X}^+\right)^\dagger$.

Analogously to the James-Cummings model's dressed state, $\hat{X}^+$ and $\hat{X}^-$ are usually called **dressed operators** and they describe the **real photons** inside the cavity, as they follow the usual definition of creation and annihilation operators. Calling the system ground state $|0\rangle$, $\langle 0|\,\hat{X}^-(t)\hat{X}^+(t)\,|0\rangle = 0$ and $\hat{X}^+|0\rangle = 0$, in contrast to $\hat{a}$ and $\hat{a}^\dagger$ that describe the **virtual photons**, as $\langle 0|\,\hat{a}^\dagger\hat{a}\,|0\rangle \neq 0$ and $\hat{a}|0\rangle \neq 0$.

Still, even if they are virtual excitations, in the sense that if we put a photodetector inside the cavity it would not detect anything except with very small probability at short timescales set by the time–energy uncertainty [42], they can have a detectable effect on different phenomena. For example, they can induce a measurable change in the Lamb shift of an ancillary probe qubit coupled to the cavity [43], and they also generate a radiation pressure in optomechanical system [44].

On the other hand, is possible to detect these excitations by converting them into real ones and there are many proposals based on different approaches, but most of them rely on a rapid modulation of either g or the atomic frequency [45, 46, 47, 48, 49] or on utilizing additional atomic levels [50, 51, 48, 52] non in USC. Both of them require USC, since these processes are not active in SC, stressing once more that USC and SC are two independent regimes [53]. Interestingly, the rapid modulation of g is connected to the dynamical Casimir effect, in which vacuum fluctuations are converted into pairs of real photons when a mirror (or another boundary condition) is moved at high speed [54, 55].

1.1.2 Violation of the gauge principle

The violation of the gauge independence principle in USC is tightly connected to the two-level approximation, a fundamental step in the derivation of the QRM. De Bernardis et al. [28] raised the question about the validity of this step, as it depended explicitly on the gauge choice once the system entered the USC regime, because in the electric

dipole gauge the two-level approximation can be performed as long as the Rabi frequency remains much smaller than the energies of all higher-lying levels, but it failed dramatically in the Coulomb gauge even for highly anharmonic spectrum above the USC threshold, as shown in Fig. 1.2 (from [28]), where the eigenvalues of the Hamiltonian without the two-level approximation (labelled full) are in perfect accordance with the Rabi Hamiltonian in the dipole gauge (H^D_{Rabi}), but deeply different from the eigenvalues of the Hamiltonian in the Coulomb gauge (H^C_{Rabi}). Still, is very well known that while choosing a different gauge leads to a different interaction form (see for example [56]), all the observable of the system must be independent of this choice, and this obviously includes eigenvalues, thus the two-level approximation seems to ruin this property.

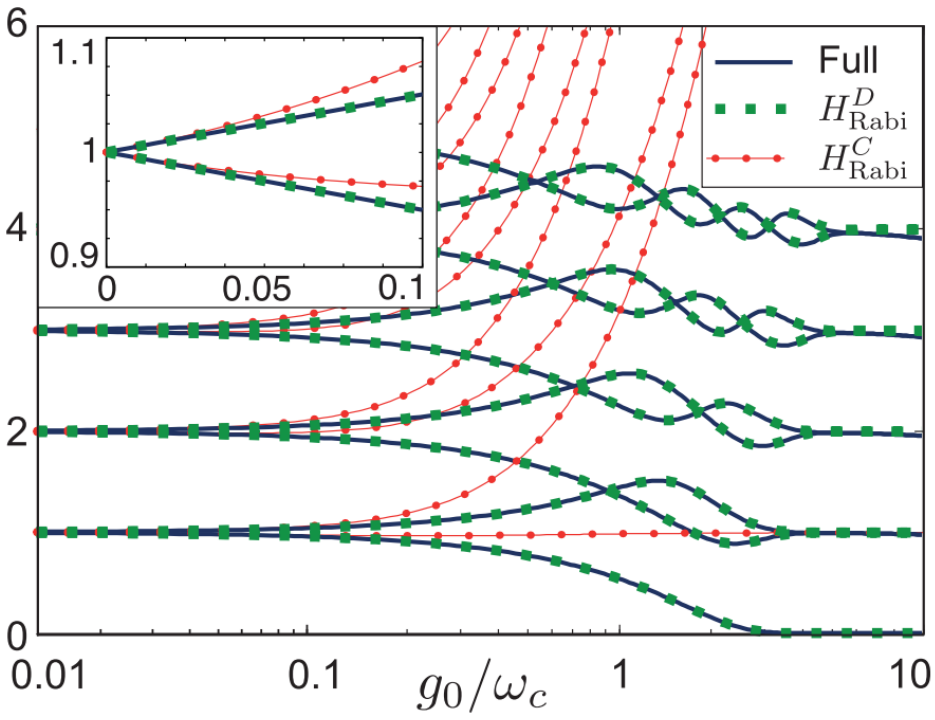

Figure 1.2: Failure of the dipole approximation in the Coulomb gauge. We see how H^C_{rabi} shows a total discordance with the full Hamiltonian in the USC regime.

At the very heart of the problem is that the derivation of the two-level Rabi Hamiltonian in the Coulomb gauge does not take into account that the truncation process can lead to a non-local potential [35], as shown by Starace in a similar problem [57], where he studied how the approximation procedure gave rise to non-local potential, causing gauge ambiguities in the calculation of atomic oscillator strength.

In order to understand why local potentials become non-local when the Hilbert space is

truncated, let us consider a one-dimensional potential $\hat{V}$. In the position basis, it can written as

$$\hat{V} = \int dx dx' \, \langle x|\hat{V}|x'\rangle \, |x\rangle\langle x'| \, . \tag{1.1.10}$$

The matrix elements of a local potential, denoted as $\langle x|\hat{V}|x'\rangle$, can be expressed as $V(x,x') = W(x)\delta(x-x')$. A complete basis is represented by $\{|n\rangle\}$ and the matrix elements can be shown as $V(x,x') = \sum_{n,n'} W_{n,n'}\psi^*_{n'}(x')\psi_n(x) = W(x)\delta(x-x')$, where we have defined $\psi_n(x)$ as $\langle x|n\rangle$. It's important to note that the Dirac delta function can only be reconstructed by retaining in its entirety the basis vectors. The two-level approximation truncates the space to only the two lowest energy levels:

$$V(x,x') \approx W_{1,0}\left[\psi^*_0(x')\psi_1(x) + \psi^*_1(x')\psi_0(x)\right] \, , \tag{1.1.11}$$

which is clearly not a reproduction of the Dirac-delta function, so the two-level approximation lead to a highly non-local potential.

A non-local potential in the position representation is described with an integral operator, that does not commute with the position operator, but it is possible to make it local by giving it a momentum dependency, $V(\hat{\mathbf{r}}, \hat{\mathbf{p}})$, as shown by several authors [57, 58, 59]. By using the translation operator $\psi(x') = e^{[i(x'-x)\hat{p}]}\psi(x)$, where $\hat{p}$ is the momentum operator, we obtain

$$\int V(x,x')\psi(x')dx' = V(x,\hat{p})\psi(x) \, . \tag{1.1.12}$$

Let's take a step back and reconsider how Hamiltonian in different gauges are obtained. The starting point is a non-relativistic quantum particle of mass m in a local potential $\boldsymbol{V}(x)$, which is described by the Hamiltonian $\hat{\mathcal{H}}_0 = q\phi(x) + \frac{1}{2m}(\hat{\boldsymbol{p}})^2 + \boldsymbol{V}(x)$. where q is the charge, $\phi(x)$ and $\boldsymbol{A}(x)$ are the scalar and vector potential. Applying the minimal coupling replacement $\boldsymbol{p} \to \boldsymbol{p} - q\boldsymbol{A}(\boldsymbol{r},t)$ ensures the gauge invariance of the Hamiltonian (see App. B for a general procedure). We still have to add the Hamiltonian of the free field, choose a gauge and quantize. If we consider the Coulomb gauge, where the particle momentum is coupled only to the transverse part of the vector potential, and consider a single-frequency cavity we obtain [56]:

$$\hat{\mathcal{H}}_C = \frac{1}{2m}(\hat{p} - q\hat{A})^2 + \hat{V}(x) + \hat{\mathcal{H}}_{ph} \, , \tag{1.1.13}$$

where $\hat{A} = A_0\left(\hat{a} + \hat{a}^\dagger\right)$ is the quantized expression for the vector potential calculated

at the particle position, A_0 is the zero-point-fluctuation amplitude and $\hat{\mathcal{H}}_{ph} = \omega_c \hat{a}^\dagger \hat{a}$ is the cavity field Hamiltonian.

The Hamiltonian in the dipole gauge, $\hat{H}_{\rm D}$, corresponds to the Power-Zienau-Woolley Hamiltonian after the dipole approximation. It can be obtained directly from the Hamiltonian in the Coulomb gauge with the electric dipole approximation (1.1.13) by means of a gauge transformation, which is also a unitary transformation: $\hat{H}_{\rm D} = \hat{U}\hat{H}_{\rm C}\hat{U}^\dagger$, where the unitary operator is $\hat{U} = \exp\left[-iqx\hat{A}/\hbar\right]$. The resulting Hamiltonian in the dipole gauge is

$$\hat{H}_{\rm D} = \hat{H}_{\rm ph} + \hat{H}_0 + \frac{q^2 A_0^2 \omega_c}{\hbar} x^2 + iq\omega_c x A_0 \left(\hat{a}^\dagger - \hat{a}\right). \tag{1.1.14}$$

Equations (1.1.13) and (1.1.14) have no gauge issue, as every observable leads to the same result.

The quantum Rabi Hamiltonian is obtained by projecting in a two-level space. Projecting (1.1.13) we obtain:

$$\hat{\mathcal{H}}'_C = \hbar\omega_c \hat{a}^\dagger \hat{a} + \frac{\hbar\omega_q}{2}\hat{\sigma}_z + \hbar g_C \sigma_y (\hat{a}^\dagger + \hat{a}) + \frac{q^2 A_0^2}{2m}(\hat{a}^\dagger + \hat{a})^2 , \tag{1.1.15}$$

where $g_C = g_D\, \omega_q/\omega_c$, while in the dipole gauge we obtain:

$$\hat{\mathcal{H}}_{\rm D} = \hat{H}_{\rm ph} + \frac{\hbar\omega_q}{2}\hat{\sigma}_z + i\hbar g_{\rm D}\left(\hat{a}^\dagger - \hat{a}\right)\hat{\sigma}_x , \tag{1.1.16}$$

where $g_{\rm D} = \omega_{\rm c} A_0 d_q/\hbar = g_{\rm C}\omega_{\rm c}/\omega_q$, and $d_q \equiv q\langle 1|x|0\rangle$ is the dipole matrix element.

Eq. (1.1.15) presents the inconsistencies expressed above because the minimal coupling replacement has been applied incorrectly. In (1.1.13) the potential has a dependency on $\hat{p}$, thus we need to apply the minimal coupling replacement. This leads to

$$\hat{\mathcal{H}}_C = \hbar\omega_c \hat{a}^\dagger \hat{a} + \frac{\hbar\omega_q}{2}\left\{\hat{\sigma}_z \cos\left[2\eta(\hat{a} + \hat{a}^\dagger)\right] + \hat{\sigma}_y \sin\left[2\eta(\hat{a} + \hat{a}^\dagger)\right]\right\} . \tag{1.1.17}$$

It is worth noting that the Hamiltonian in both gauges can be rewritten in a similar way to the non-interacting Hamiltonian, given that we redefine the system operators, the matter ones for the dipole gauge and the photonic one for the Coulomb gauge. To show this we consider that eq. (1.1.17), the correct Rabi Hamiltonian in the Coulomb gauge, can be written as the sum of the free photonic field $\hat{H}_c$ (1.1.3) and an interacting matter contribution obtained by applying the unitary transformation $\hat{U}$ to the free matter Hamiltonian $\hat{H}_q$ (1.1.1) [60]:

$$\hat{\mathcal{H}}_C = \hat{\mathcal{H}}_c + \hat{U}^\dagger \hat{\mathcal{H}}_q \hat{U} . \tag{1.1.18}$$

Introducing the Coulomb-gauge Pauli operators [61]

$$\hat{\sigma}'_z = \hat{U}^\dagger \hat{\sigma}_z \hat{U}^\dagger = \hat{\sigma}_z \cos\left[2\eta\left(\hat{a}^\dagger + \hat{a}\right)\right] + \hat{\sigma}_y \sin\left[2\eta\left(\hat{a}^\dagger + \hat{a}\right)\right], \tag{1.1.19}$$

the Hamiltonian in (1.1.15) can be rewritten in a more compact way as:

$$\hat{\mathcal{H}}_C = \hat{\mathcal{H}}_c^{(0)} + \frac{\omega_q}{2}\hat{\sigma}'_z \,. \tag{1.1.20}$$

As a consequence, the dipole gauge Hamiltonian can be directly obtained as

$$\hat{H}_D = \hat{U}\hat{H}_C\hat{U}^\dagger = \hat{U}\hat{H}_c\hat{U}^\dagger + \hat{H}_q \,. \tag{1.1.21}$$

The result is

$$\hat{\mathcal{H}}_D = \hat{\mathcal{H}}_c^{(0)} + \hat{\mathcal{H}}_q^{(0)} + \hat{\mathcal{V}}_D^{\mathrm{cq}} \,, \tag{1.1.22}$$

where the interaction term is

$$\hat{\mathcal{V}}_D^{\mathrm{cq}} = i\eta\omega_c\left(\hat{a}^\dagger - \hat{a}\right)\hat{\sigma}_x + \eta^2\omega_c\,\hat{\sigma}_x^2 \,, \tag{1.1.23}$$

being η the normalized qubit-cavity coupling strength and $\hat{\sigma}_x^2 = \hat{I}$ just corresponds to the identity operator. Introducing the dipole gauge photon operators [61]

$$\begin{aligned} \hat{a}' &= \hat{\mathcal{T}}\hat{a}\hat{\mathcal{T}}^\dagger = \hat{a} + i\eta\hat{\sigma}_x \,, \\ \hat{a}'^\dagger &= \hat{\mathcal{T}}\hat{a}^\dagger\hat{\mathcal{T}}^\dagger = \hat{a}^\dagger - i\eta\hat{\sigma}_x \,, \end{aligned} \tag{1.1.24}$$

(1.1.22) can be written as

$$\hat{\mathcal{H}}_D = \omega_c\hat{a}'^\dagger\hat{a}' + \hat{\mathcal{H}}_q^{(0)} \,. \tag{1.1.25}$$

Equations (1.1.18) and (1.1.21) show that, in general, while the Coulomb gauge can be correctly implemented by applying a unitary transformation (generalized minimal coupling replacement) to the bare matter Hamiltonian, the dipole gauge Hamiltonian can be obtained by applying a generalized minimal coupling replacement (with opposite coupling constant) to the free-field Hamiltonian. The form of the operators in the two gauges are summarized in the table 1.1.

Of course, the two gauges, being related by a unitary transformation, provide the same physical results [61]. We also notice that, while the correct Coulomb-gauge quantum Rabi Hamiltonian is very different from the corresponding standard quantum Rabi Hamiltonian [28, 35], the standard dipole gauge model is not affected by gauge issues as shown by (1.1.22).

Dipole gauge	Coulomb gauge
$\hat{a}_D = \hat{a}' = \hat{a} + i\eta\hat{\sigma}_x$	$\hat{a}_C = \hat{a}$
$\hat{a}_D^\dagger = \hat{a}'^\dagger = \hat{a}^\dagger - i\eta\hat{\sigma}_x$	$\hat{a}_C^\dagger = \hat{a}^\dagger$
$\sigma_x^D = \sigma_x$	$\sigma_x^C = \sigma_x$
$\sigma_y^D = \sigma_y$	$\sigma_y^C = \sigma_y' = \hat{\sigma}_y \cos\left[2\eta\left(\hat{a}^\dagger + \hat{a}\right)\right] - \hat{\sigma}_z \sin\left[2\eta\left(\hat{a}^\dagger + \hat{a}\right)\right]$
$\sigma_z^D = \sigma_z$	$\sigma_z^C = \sigma_z' = \hat{\sigma}_z \cos\left[2\eta\left(\hat{a}^\dagger + \hat{a}\right)\right] + \hat{\sigma}_y \sin\left[2\eta\left(\hat{a}^\dagger + \hat{a}\right)\right]$

Table 1.1: Atomic and photonic operators in dipole and Coulomb gauge

1.1.3 Decoupling

Another feature of the Rabi model worth mentioning is the decoupling [62], a characteristic feature of the DSC regime, where the light-matter system for high coupling value lose its dependency on the coupling strength, acting as it is effectively decoupled. As shown in Fig. 1.2, for $\eta \to \infty$ the eigenvalues have a pairwise degeneration and their value corresponds to that for $\eta = 0$. A further indication of the inadequacy of the H_{Rabi}^C is its failure to exhibit decoupling.

We start considering $\hat{\mathcal{H}}_D$ (1.1.22):

$$\hat{\mathcal{H}}_D = \frac{\omega_q}{2}\hat{\sigma}_z + \omega_c \hat{a}'^\dagger \hat{a}' \,. \tag{1.1.26}$$

We recall Eqs. (1.1.24):

$$\begin{aligned} \hat{a}' &= \hat{a} + i\eta\hat{\sigma}_x \,, \\ \hat{a}'^\dagger &= \hat{a}^\dagger - i\eta\hat{\sigma}_x \,. \end{aligned} \tag{1.1.27}$$

When $\eta\omega_c \gg \omega_q$, the term $\frac{\omega_q}{2}\hat{\sigma}_z$ can be treated as a perturbation and can be neglected in the limit $\eta \to \infty$. The resulting Hamiltonian commutates with $\hat{\sigma}_x$, thus we can project it into the eigenstates of $\hat{\sigma}_x$ ($|\pm\rangle$):

$$\hat{\mathcal{H}}_D \to \hat{\mathcal{H}}_{D\pm}^\infty = \omega_c \hat{a}_\pm'^\dagger \hat{a}_\pm' \,, \tag{1.1.28}$$

where we have now defined:

$$\begin{aligned} \hat{a}_\pm' &= \hat{a} \pm i\eta \,, \\ \hat{a}_\pm'^\dagger &= \hat{a}^\dagger \mp i\eta \,. \end{aligned} \tag{1.1.29}$$

The operators $\hat{a}_\pm'$ and $\hat{a}_\pm'^\dagger$ are just bare creation and annihilation operators $\hat{a}^\dagger$ and $\hat{a}$ displaced by a quantity $\pm i\eta$. By using the displacement operator $\hat{D}(\alpha) = \exp\left(\alpha\hat{a}^\dagger - \alpha^*\hat{a}\right)$ (in our case $\alpha = \pm i\eta$), the unitary condition $\hat{D}(\alpha)\hat{D}^\dagger(\alpha) = \hat{D}^\dagger(\alpha)\hat{D}(\alpha) = \hat{1}$ and

$\hat{D}^\dagger(\alpha) = \hat{D}(-\alpha)$, it can be shown that (1.1.28) corresponds to the Hamiltonian of a displaced anharmonic oscillator:

$$\hat{\mathcal{H}}^{\infty}_{D\pm} = D(\pm i\eta)\left(\omega_c \hat{a}^\dagger \hat{a}\right)\hat{D}^\dagger(\pm i\eta)\,. \tag{1.1.30}$$

Since the transformation $\hat{D}(\pm i\eta)$ is unitary, it does not affect the eigenvalues. Hence, in the limit $\eta \to \infty$, the eigenvalues of $\hat{\mathcal{H}}_D$ are those of the anharmonic oscillator $\hat{\mathcal{H}}_c^- = \omega_c \hat{a}^\dagger \hat{a}$.

It is worth noticing that this is a general behaviour of generalized QRMs satisfying the gauge principle. Specifically, it can be applied to every general quantum Rabi Hamiltonian, whose expression is,

$$\hat{\mathcal{H}}_{Dipole} = \frac{\omega_q}{2}\hat{\sigma}_z + \omega_c \hat{a}'^\dagger \hat{a}' + \hat{V}\,, \tag{1.1.31}$$

as long as $\left[\hat{V}, \hat{\sigma}_x\right] = 0$.

Chapter 2

Non Linear oscillator

In this chapter, we investigate the gauge issues arising from considering a generalized QRM with a non-linear electromagnetic resonator and how an incorrect application of the minimal coupling replacement, will exacerbate the issue presented in the previous chapter. We will show a simple model for a non-linear electromagnetic resonator, a polaritonic model to obtain the correct form of interaction and combine this result with the one presented in the previous chapter to obtain a consistent expansion of the QRM to non-linear systems. These results are published in [63] and all the figures in this chapter were originally published there.

2.1 Simple models for the non-linear electromagnetic resonator

Let us consider a general Hamiltonian of a single-mode electromagnetic resonator with a non-linear self-interaction:

$$\hat{\mathcal{H}}_{c,\alpha} = \hat{H}_c^{(0)} + \hat{\mathcal{V}}_\alpha \,, \tag{2.1.1}$$

where $H_c^{(0)} = \omega_c \hat{a}^\dagger \hat{a}$ is the harmonic term.

We are going to consider different interaction Hamiltonians and compare their results. A widely used non-linear Hamiltonian that shows a third-order anharmonicity self-interaction term is the Kerr Hamiltonian ($\alpha = k$)

$$\hat{\mathcal{H}}_{c,k} = \omega_c \hat{a}^\dagger \hat{a} + J\, \omega_c\, \hat{a}^{\dagger 2}\, \hat{a}^2 \,. \tag{2.1.2}$$

This term is obtained by applying the RWA to the more general interaction ($\alpha = \pm$)

$$\hat{\mathcal{H}}_{c,\pm} = \omega_c \hat{a}^\dagger \hat{a} + \frac{J\omega_c}{6}(\hat{a}^\dagger \pm \hat{a})^4 \,. \tag{2.1.3}$$

When the resonator interacts with qubits in the strong coupling regime, the photon operator $\hat{a}$ ($\hat{a}^\dagger$) may contain also negative (positive) frequency components. As a consequence, a more careful RWA has to be applied.

Finding a precise formulation for the non-linear potential operator, denoted as $\hat{\mathcal{V}}_{\rm nl}$, is a complex undertaking. The likelihood of photons interacting with each other in a vacuum is incredibly low, which means that non-linear optical phenomena require the interaction of photons and matter. The Kerr effect, among other effective photon-photon interactions, emerges from the interaction of photons in a spectral range that corresponds to the transparency window of a medium in the dispersive regime. To obtain a Hamiltonian for a non-linear optical resonator, one can follow a straightforward approach. This involves examining the classical representation of the electromagnetic field's energy density within a dielectric medium.

The contribution arising from the interaction with the medium is

$$U = \frac{1}{2}\,\mathbf{E}\cdot\mathbf{P}\,, \tag{2.1.4}$$

where $\mathbf{E}$ is the electric field, and $\mathbf{P}$ is the polarization density.

The polarization induced in a medium can be expanded in a power series in the electric field, with the third order non-linear polarization expressed as $P_i^{(3)} = \chi_{ijkl}^{(3)} E_j E_k E_l$, where $\chi^{(3)}$ is the third-order non-linear optical susceptibility tensor. This implies that the contribution of non-linear processes to the total field energy is proportional to the fourth power of the electric field.

In the case of a single-mode electromagnetic resonator, the vector potential amplitude can be expanded as $\hat{A} = A_0(\hat{a} + \hat{a}^\dagger)$, where A_0 is the zero-point-amplitude of the field coordinate and $\hat{a}$ and $\hat{a}^\dagger$ are the destruction and creation photon operators, and the amplitude electric field operator can be written as $\hat{E} = i\omega_c A_0(\hat{a} - \hat{a}^\dagger)$. This leads to a non-linear interaction term proportional to the fourth power of the electric field operator, $\hat{\mathcal{V}}_- = (J\omega_c/6)(\hat{a} - \hat{a}^\dagger)^4$. However, a more rigorous microscopic approach is needed to eliminate any concerns, so in section 2.2, we will present a simple microscopic model able to provide indications on the right choice for the effective non-linear potential.

One interesting point to make note of is that $\hat{\mathcal{V}}_+$ and $\hat{\mathcal{V}}_-$ are related by the unitary transformation $\hat{a} \rightarrow i\hat{a}$. This transformation will not change the linear term $\hat{H}_c^{(0)}$, but will change other quantities such as the vector potential $\hat{A}$. Although these two options yield the same output for any single non-linear optical resonator described by the Hamiltonian in (2.1.1), they may produce dissimilar outcomes when combined with an additional system, such as a qubit.

To gain a more detailed understanding of the system, it is helpful to compare the lowest energy eigenvalue of $\hat{\mathcal{H}}_{c,K}$ with those of $\hat{\mathcal{H}}_{c,\pm}$ (Fig. 2.1 where we set to zero the energy of the ground state for each value of J). Since changing the parameter J affects the transition frequency between the first excited state and the ground state only of $\hat{\mathcal{H}}_{c,\pm}$, the frequency ω_c in $\hat{\mathcal{H}}_{c,\pm}$ is modified as a function of J, so that these transition frequencies do coincide.

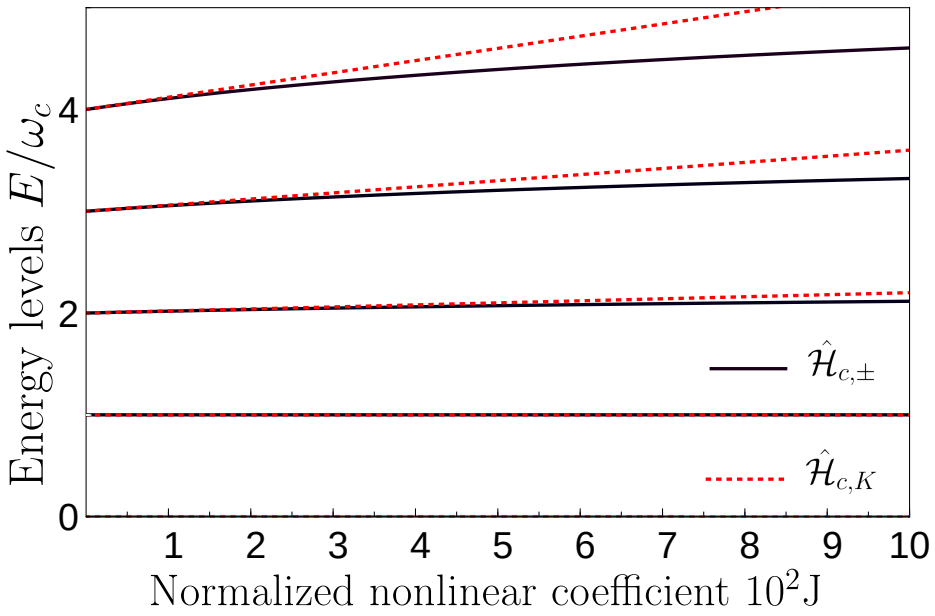

Figure 2.1: Comparison between the lowest-energy eigenvalues of the non-linear Hamiltonians $\hat{\mathcal{H}}_{c,\pm}$ and $\hat{\mathcal{H}}_{c,K}$ as function of the normalized non-linear coefficient J. We assume the respective ground state energy equal to zero at each value of J. The bare cavity frequency ω_c is opportunely renormalized as a function of J in the Hamiltonians $\hat{\mathcal{H}}_{c,\pm}$ so that transition frequency between the first excited state and the ground state do coincide to that calculated for the non-linear Kerr Hamiltonian $\hat{\mathcal{H}}_{c,K}$.

2.2 Polariton model of the non-linear resonator

In this section we present a polariton model to discern the correct form for the non-linear interaction between $\hat{\mathcal{H}}_{c,\pm}$.

As mentioned before, since is extremely unlikely that photons interact with each other, we considered that the non-linearity comes from the interaction with an optically active medium placed inside the cavity. The medium is modelled as an additional bosonic field describing the collective electronic excitations, coupled in the dispersive regime. In the dispersive regime we can identify two polaritons, one corresponding to the cavity mode dressed by the interaction, and the other to the dressed matter field.

Neglecting the non-linear potential of the matter field allows us to exactly diagonalize the resulting Hopfield model. Then, we add the non-linear term and express it in terms of the polariton operators, effectively modelling the non-linear cavity.

The resulting Hamiltonian for a single-mode electromagnetic resonators interacting with a single-mode bosonic collective matter excitation in the dipole gauge [64] is:

$$\hat{\mathcal{H}}_D = \hat{\mathcal{H}}_c^{(0)} + \hat{\mathcal{H}}_b^{(0)} + \hat{\mathcal{V}}_{cb}\,, \tag{2.2.1}$$

where the non-interacting contributions are $\hat{\mathcal{H}}_c^{(0)} = \omega_0 \hat{a}^\dagger \hat{a}$, $\hat{\mathcal{H}}_b^{(0)} = \omega_c \hat{b}^\dagger \hat{b}$, and the interaction term is

$$\hat{\mathcal{V}}_{cb} = \omega_0 \left[i\lambda(\hat{a}^\dagger - \hat{a})(\hat{b} + \hat{b}^\dagger) + \lambda^2(\hat{b} + \hat{b}^\dagger)^2 \right]. \tag{2.2.2}$$

This Hamiltonian can be diagonalized by an Hopfield-Bogoliubov transformation [65] (see App.A for details):

$$\hat{a} = \sum_{n=1,2} A_n \hat{P}_n + A'_n \hat{P}_n^\dagger\,, \tag{2.2.3}$$

and

$$\hat{b} = \sum_{n=1,2} B_n \hat{P}_n + B'_n \hat{P}_n^\dagger\,, \tag{2.2.4}$$

where $\hat{P}_n$ and $\hat{P}_n^\dagger$ $(n = 1, 2)$ are the lower $(n = 1)$ and upper $(n = 2)$ polariton (bosonic) operators, and A_n, A'_n, B_n, B'_n are complex numbers that can be obtained through the Hopfield-Bogoliubov diagonalization procedure (see Appendix A for their explicit form). The resulting diagonal form can be written as:

$$\hat{\mathcal{H}}_D = \sum_{n=1,2} \omega_n \hat{P}_n^\dagger \hat{P}_n\,. \tag{2.2.5}$$

and ω_n can be obtained from the dispersion relation

$$1 + \frac{4\lambda^2 \omega_0 \omega_c}{\omega_0^2 - \omega_n^2} = \frac{\omega_c^2}{\omega_n^2}. \tag{2.2.6}$$

Using the expressions (2.2.3) and (2.2.4), is possible to obtain the explicit form for the polariton operators in terms of the bare photon and matter operators:

$$\hat{P}_n = A_n^* \hat{a} + B_n^* \hat{b} - A_n' \hat{a}^\dagger - B_n' \hat{b}^\dagger. \tag{2.2.7}$$

Given (2.2.3),(2.2.4) and (2.2.7), we can obtain an explicit expression for the non-linear term of (2.1.3). Assuming an even potential, the lowest order above the harmonic potential is the fourth power of the matter field coordinate $\hat{x}^4$, where $\hat{x} = x_0(\hat{b} + \hat{b}^\dagger)$, being x_0 the zero-point-fluctuation amplitude. The total system Hamiltonian can be expressed as

$$\hat{\mathcal{H}} = \hat{\mathcal{H}}_D + \frac{J_b \omega_c}{6}(\hat{b} + \hat{b}^\dagger)^4 \,, \tag{2.2.8}$$

that in terms of the polariton operators is:

$$\hat{b} + \hat{b}^\dagger = \sum_n \left(B_n + B_n'^* \right) \hat{P}_n + \text{h.c.}\,. \tag{2.2.9}$$

By inspecting the phases and moduli of the Hopfield coefficients (see Appendix A.1), the non-linear term in (2.2.8) can be written as

$$\begin{aligned} \hat{\mathcal{H}} =& \omega_1 \hat{P}_1^\dagger \hat{P}_1 + \omega_2 \hat{P}_2^\dagger \hat{P}_2 + \\ &+ \frac{J_b}{6} \left[i C_1 \left(\hat{P}_1 - \hat{P}_1^\dagger \right) + C_2 \left(\hat{P}_2 + \hat{P}_2^\dagger \right) \right]^4 \,, \end{aligned} \tag{2.2.10}$$

where $C_n = |B_n|\left[2\omega_0/(\omega_n + \omega_0)\right]$.

Considering that we are in the dispersive regime, is possible to neglect the contribution coming from the upper polariton, since, when the detuning $|\Delta| \gg \omega_0 \lambda$, light-matter hybridization is rather small. This means that one polariton can be interpreted as a dressed photon mode, since its eigenfrequency will be close to the one of the bare photon, while the other as a dressed matter mode, with an eigenfrequency close to the one of the bare matter field. This latter interpretation is also supported by the fact that the polariton quanta are those really detected in photo-detection measurements [66].

When describing processes and experiments occurring in a spectral range well separated by ω_b, it is possible to discard the contributions of the matter-like polariton. Assuming $\omega_b > \omega_c$, the resulting approximate Hamiltonian is

$$\hat{\mathcal{H}}_{D,1} = \omega_1 \hat{P}_1^\dagger \hat{P}_1 + \frac{J\omega_c}{6}\left(\hat{P}_1 - \hat{P}_1^\dagger\right)^4 , \tag{2.2.11}$$

with $J = J_b(C_1)^4$. The polariton operators P_1 and $P_1^\dagger$ can be interpreted as photon operators exhibiting non-linear self-interaction caused by their interaction with the matter field. This interaction has resulted in a frequency shift from $\omega_c \to \omega_1 \simeq \omega_c$, as well as an effective non-linear self-interaction.

This result shows that the correct interaction form in (2.1.3) is $\hat{\mathcal{V}}_{nl-} = J\omega_c(\hat{a} - \hat{a}^\dagger)^4$, where the photon operator $\hat{a}$ actually corresponds to the polariton operator $\hat{P}_1$.

2.3 Non-linear-resonator quantum Rabi model

In this section we will study the interaction of a qubit with the non-linear oscillator presented in Section 2.1.

All the calculations will be in the dipole gauge since the Hamiltonian will have a simpler form.

The immediate way to obtain the Hamiltonian for the system would be to just add the non-linear potential to the Rabi Hamiltonian (1.1.16):

$$\hat{\mathcal{H}}_{sD}^{\alpha} = \hat{\mathcal{H}}_D + \hat{\mathcal{V}}_\alpha \, . \tag{2.3.1}$$

Yet, this simple Hamiltonian violates the gauge principle since $\hat{\mathcal{V}}_\alpha$ does not commute with $\hat{\mathcal{U}}$ ($\alpha \neq \pm$). In fact, transforming (2.3.1) to obtain the Coulomb gauge Hamiltonian, we obtain a result which differs from the minimal coupling:

$$\hat{\mathcal{U}}\hat{\mathcal{H}}_{sD}^{\alpha}\hat{\mathcal{U}}^\dagger = \hat{\mathcal{H}}_C + \hat{\mathcal{U}}\hat{\mathcal{V}}_\alpha\hat{\mathcal{U}}^\dagger \neq \hat{\mathcal{H}}_{c,\alpha} = \hat{\mathcal{H}}_C + \hat{\mathcal{V}}_\alpha \, . \tag{2.3.2}$$

The correct procedure to obtain a gauge-independent Hamiltonian is to apply the minimal coupling replacement, shown in (1.1.21). This leads to:

$$\hat{\mathcal{H}}_D^{\alpha} = \hat{\mathcal{U}}^\dagger \hat{\mathcal{H}}_{c,\alpha}\hat{\mathcal{U}} + \hat{\mathcal{H}}_q^{(0)} \, . \tag{2.3.3}$$

As shown in Sec. 1.1.2, applying the minimal coupling replacement is equivalent to transforming all the photonic operators in the non-interacting Hamiltonian through the transformation (1.1.24).

But, this transformation only modify $\hat{\mathcal{V}}_-$ and $\hat{\mathcal{V}}_K$, while it commutes with $\hat{\mathcal{V}}_+$, thus leaves it unaffected. For this exact reason it is imperative to consider the microscopic model presented in Sec. 2.2 to choose the correct form for the Hamiltonian, since the three potentials $\hat{\mathcal{V}}_+$, $\hat{\mathcal{V}}_-$ and $\hat{\mathcal{V}}_K$ provides gauge independent results.

2.4 Energy spectra of non-linear-resonator quantum Rabi models

Here we present a set of numerical calculations clarifying the impact of using the different models above described, and the impact on the energy spectra of violating gauge invariance. We will compare the five different Hamiltonians illustrated previously, the two non gauge invariant $\hat{\mathcal{H}}_{sD}^{-}$, $\hat{\mathcal{H}}_{sD}^{K}$ and the other three that satisfy the gauge principle $\hat{\mathcal{H}}_{D}^{-}$, $\hat{\mathcal{H}}_{D}^{+}$ and $\hat{\mathcal{H}}_{D}^{K}$. As proven in Sec. 2.2 we know that the correct non-linear interaction term has a minus sign, so the correct Hamiltonian describing this system is $\hat{\mathcal{H}}_{D}^{-}$, yet, it may be beneficial to compare the energy eigenvalues of the different Hamiltonians to determine the impact of using an incorrect non-linear photonic potential.

Let us start with a comparison between the two non-gauge invariant Hamiltonians $\hat{\mathcal{H}}_{sD}^{-}$ and $\hat{\mathcal{H}}_{sD}^{K}$ and $\hat{\mathcal{H}}_{D}^{-}$. Fig. 2.2 show the eigenvalues as function of the normalized coupling strength η with no detuning, $\omega_q/\omega_c = 1$. We present two specific values of the normalized non-linear coefficient $J = 0.05$ (a) and $J = 0.1$ (b).

The first problem that we see with the two gauge dependant Hamiltonians $\hat{\mathcal{H}}_{sD}^{-}$ and $\hat{\mathcal{H}}_{sD}^{K}$ is that there is no decoupling. As expressed in Sec. 1.1.3, one notable aspect of the QRM is that when $\eta \gg 1$, the bare energy of the qubit can be viewed as a minor perturbation. As η approaches infinity, this perturbation becomes insignificant in comparison to the interaction term, leading to a pairwise degeneration of the eigenvalues. This phenomenon results in the QRM displaying the same energy levels as it would at zero coupling ($\eta = 0$) when this perturbation becomes insignificant. Yet, only the eigenvalues of $\hat{\mathcal{H}}_{D}^{-}$ exhibit this tendency, as they become uncorrelated with η.

We also observe that the region where the eigenvalues of $\hat{\mathcal{H}}_{sD}^{-}$ and $\hat{\mathcal{H}}_{sD}^{K}$ agree with those of $\hat{\mathcal{H}}_{D}^{-}$ is very limited around very low coupling values and for the lowest energy levels.

Moving to the analysis of the gauge independent Hamiltonians, Fig. 2.3 shows the comparison between $\hat{\mathcal{H}}_{D}^{-}$, $\hat{\mathcal{H}}_{D}^{+}$ and $\hat{\mathcal{H}}_{D}^{K}$. We fixed the same parameters as before, zero-

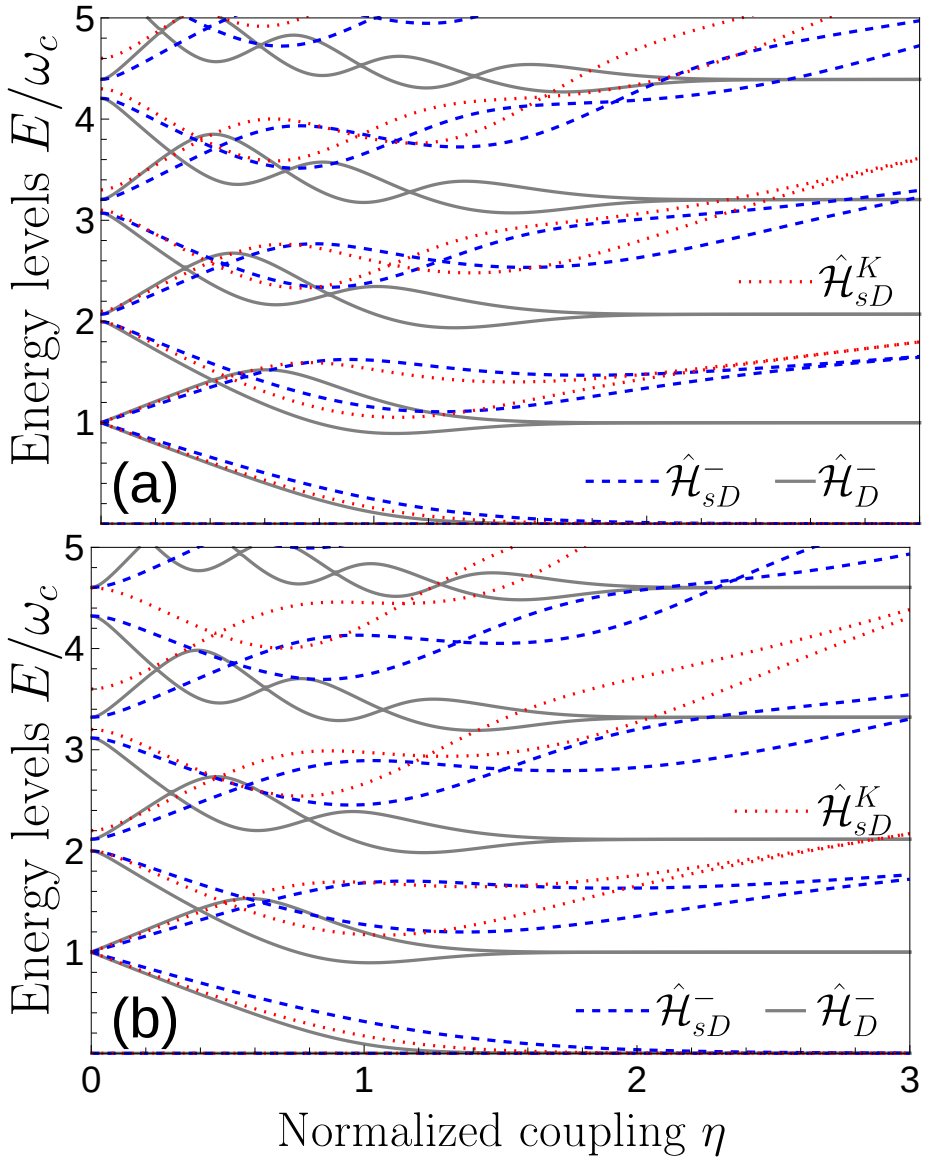

Figure 2.2: Comparison of the lowest energy eigenvalues of the Hamiltonians $\hat{\mathcal{H}}^-_{sD}$, $\hat{\mathcal{H}}^K_{sD}$ and $\hat{\mathcal{H}}^-_D$, as function of the resonator-qubit normalized coupling η, for (a) $J = 0.05$ and (b) $J = 0.1$. The eigenvalues of $\hat{\mathcal{H}}^-_{sD}$, $\hat{\mathcal{H}}^K_{sD}$ and $\hat{\mathcal{H}}^-_D$ are compared setting at zero the respective ground state energy at each value of η.

detuning ($\omega_q/\omega_c = 1$) and normalized non-linear coefficient $J = 0.05$ (a) and $J = 0.1$ (b).

When analyzing the behaviour of all three elements at high coupling, one can observe the light-matter decoupling, as they gradually become independent of η. This observation emphasizes the importance of adhering to the gauge principle, which ensures consistent outcomes at higher coupling strengths. Additionally, it is worth noting that the eigenvalues of $\hat{\mathcal{H}}_D^+$ start to exhibit a decoupling effect at slightly higher η values. Furthermore, the eigenvalues of $\hat{\mathcal{H}}_D^K$ demonstrate the most significant discrepancies in comparison to those of $\hat{\mathcal{H}}_D^-$, particularly in the energy levels of the excited states at $\eta = 0$. When the normalized non-linear coefficient is increased to $J = 0.1$ [refer to Fig. 2.3 (b)], the distinctions become more prominent. Even the fourth excited eigenvalues of the three Hamiltonians present notable differences, even at coupling strengths that are considered moderate.

This is an extremely important result as the non-linearity shows how important it is to have a consistent Hamiltonian that satisfies the gauge principle. While usually the contribution shown in sec. 1.1.2 can be discarded outside the USC, here we show how it is not always the case. Additionally, the specific range of validity of the standard Kerr model depends on the normalized coefficient J of the photonic non-linearity, on the qubit-oscillator normalized coupling strength η, and on the considered energy levels, as shown in Fig. 2.3.

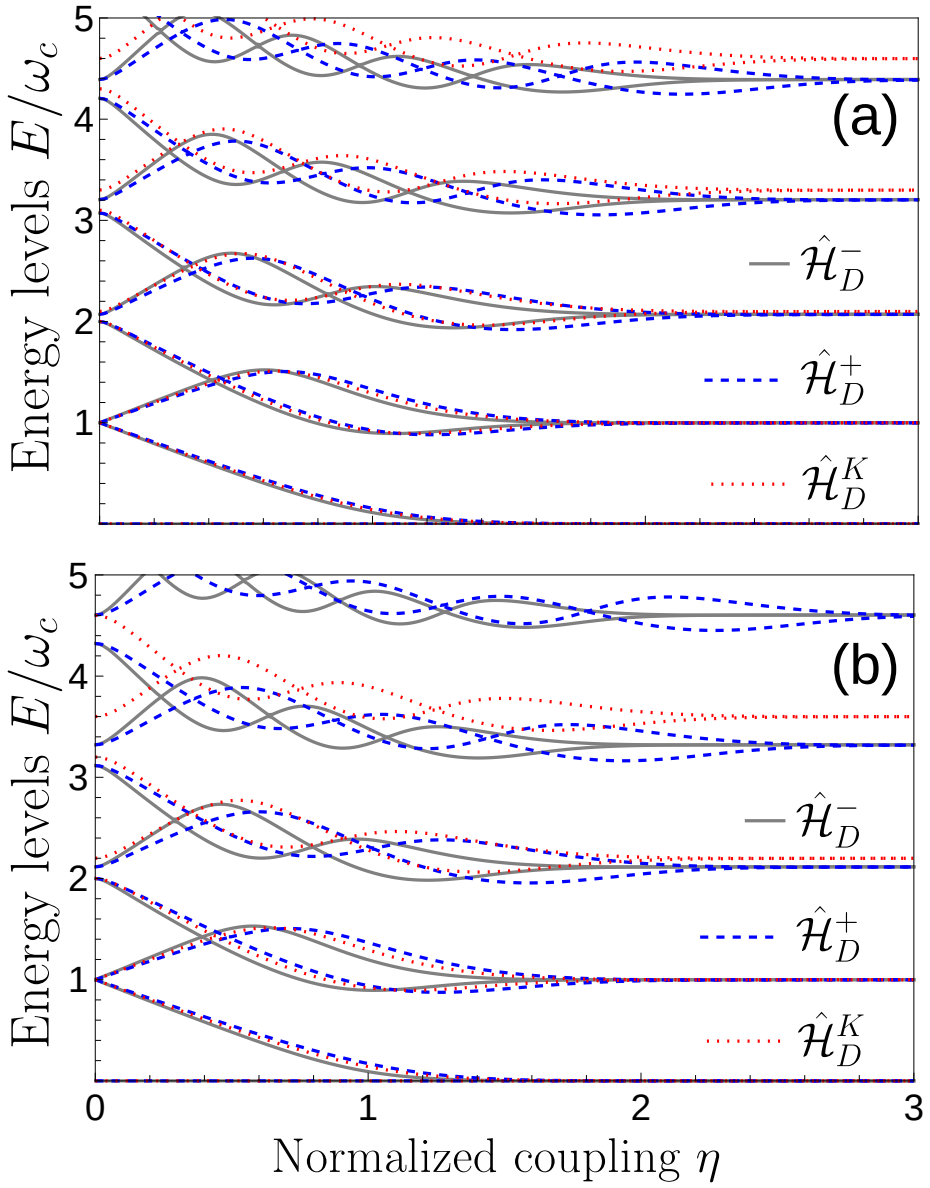

Figure 2.3: Comparison between the lowest energy energy levels of $\hat{\mathcal{H}}_D^{\pm}$, and $\hat{\mathcal{H}}_D^K$ as function of the normalized coupling η for (a) $J = 0.05$ and (b) $J = 0.1$. The eigenvalues of $\hat{\mathcal{H}}_D^{\pm}$ and $\hat{\mathcal{H}}_D^K$ are compared assuming the respective ground state energy equal to zero at each value of η.

Chapter 3

Dephasing

Dephasing is a phenomenon that occurs in quantum systems when they interact with their environment and lose their coherence. As no quantum system can be considered isolated from its environment, dephasing gives us a time scale for the "quantumness" of a system, since coherence is the property of quantum systems that allows them to exist in superpositions of states and exhibit interference effects and the dephasing is the process that destroys these quantum features and makes the system behave more classically [67, 7]. Dephasing is important for understanding the limitations of quantum technologies, such as quantum computing and quantum metrology, as well as the fundamental aspects of quantum physics, such as the measurement problem and the emergence of classicality. Since the decoherence time increases with the dimension of the system [68], it is clear why is so hard to see quantum effects in the macroscopic scale [69]. Yet, decoherence is not always a detrimental factor, as it has been shown that pure dephasing is a promising resource for solid-state emitters since it can improve the performance of nanophotonic devices, such as single-photon sources and nanolasers [70]. Considering the widespread interest in using quantum effects to build either more efficient devices or entirely new devices it is clear the importance of a correct description for this phenomenon.

In this chapter, we show how to correctly describe a stochastic perturbation describing the dephasing of one of the system's components, depending on the adopted gauge. We find that neglecting the modification on the operators describing the dephasing caused by choosing a gauge leads to unphysical and wrong results in both USC and DSC. These results are published in [71], and all the figures in this chapter were originally published there.

3.1 Quantum Rabi model

We will start our discussion by pointing out that the interaction between light and matter can significantly affect the form of a stochastic perturbation describing the dephasing of one of the components. Neglecting this issue can lead to wrong and unphysical results in both USC and DSC regimes. To show this, we consider that dephasing effects on both the qubit and electromagnetic field can be described by introducing two zero-mean stochastic functions $f_c(t), f_q(t)$ modulating their resonance frequency. The perturbation Hamiltonian can be written as

$$\hat{\mathcal{V}}_{\rm dep} = \hat{\mathcal{V}}^c_{\rm dep} + \hat{\mathcal{V}}^q_{\rm dep} = f_c(t)\hat{a}^\dagger\hat{a} + f_q(t)\sigma_z\,. \tag{3.1.1}$$

Usually, the decoherence in hybrid quantum systems is described by using a master equation approach [46, 72], by expanding the perturbation $\hat{\mathcal{V}}_{\rm dep}$ in the basis of the eigenstates of the total system Hamiltonian and moving to the interaction picture, we obtain:

$$\hat{\mathcal{V}}_{\rm dep}(t) = f_q(t)\sum_{j,k}\langle j|\hat{\sigma}_z|k\rangle\,|j\rangle\langle k|\,e^{i\omega_{jk}t} + f_c(t)\sum_{j,k}\langle j|\hat{a}^\dagger\hat{a}|k\rangle\,|j\rangle\langle k|\,e^{i\omega_{jk}t}\,, \tag{3.1.2}$$

where $|j\rangle$ are the eigenstates of the total Hamiltonian and ω_{jk} are the transition frequencies. Using the Fourier decomposition of $f(t)$, and assuming that the main contribution to dephasing results from a small frequency interval around ω_{jk}, we obtain:

$$\hat{\mathcal{V}}_{\rm dep}(t) = \sum_{j,k}\hat{\sigma}_z^{jk}\,|j\rangle\langle k|\,f^{(q)}_{-\omega_{jk}}(t) + \sum_{j,k}\langle j|\hat{a}^\dagger\hat{a}|k\rangle\,|j\rangle\langle k|\,f^{(c)}_{-\omega_{jk}}(t)\,, \tag{3.1.3}$$

where

$$f^{(x)}_{\omega_{jk}}(t) = \sqrt{S^{(x)}_f(\omega_{jk})}\xi_{\omega_{jk}}(t)\,, \tag{3.1.4}$$

with $x = q, c$, $S^{(x)}_f(\omega)$ is the spectral density of $f^{(x)}(t)$, and, since are assuming a white noise, the condition on $\xi(\omega)$ are $\langle\xi(\omega)\rangle = 0$ and $\langle\xi(\omega)\xi(\omega')\rangle = \delta(\omega-\omega')$. If the transition frequencies ω_{jk} are well-separated, we can treat each term of the above summation as an independent noise.

The resulting master equation (ME) can be written as ($\hbar = 1$) [73]:

$$\frac{d}{dt}\hat{\rho}(t) = -i[\hat{H}_s, \hat{\rho}] + \mathcal{L}_{\rm dr}\hat{\rho}\,, \tag{3.1.5}$$

where $\hat{H}_s$ is the Hamiltonian of the total system and $\mathcal{L}_{\mathrm{c,q}}\hat{\rho}$ is the Lindblad dissipator:

$$\mathcal{L}_{\mathrm{dr}}\cdot = \mathcal{D}\left[\sum_j \Phi^j \left|j\right\rangle\!\left\langle j\right|\right]\cdot + \sum_{j,k\neq j} \Gamma_\phi^{jk}\,\mathcal{D}\left[\left|j\right\rangle\left\langle k\right|\right]\cdot \ , \tag{3.1.6}$$

where

$$\mathcal{D}[\hat{O}]\hat{\rho} = \frac{1}{2}(2\hat{O}\hat{\rho}\hat{O}^\dagger - \hat{\rho}\hat{O}^\dagger\hat{O} - O^\dagger\hat{O}\hat{\rho}) \tag{3.1.7}$$

is the Lindbladian superoperator,

$$\Phi^j = \sqrt{\frac{\gamma_\phi^{(q)}(0)}{2}}\sigma_z^{jj} + \sqrt{\frac{\gamma_\phi^{(c)}(0)}{2}}\left\langle j|\hat{a}^\dagger\hat{a}|j\right\rangle, \tag{3.1.8}$$

and

$$\Gamma_\phi^{jk} = \frac{\gamma_\phi^{(q)}(\omega_{kj})}{2}\left|\sigma_z^{jk}\right|^2 + \frac{\gamma_\phi^{(c)}(\omega_{kj})}{2}\left|\left\langle j|\hat{a}^\dagger\hat{a}|k\right\rangle\right|^2 \ . \tag{3.1.9}$$

The bare dephasing rates $\gamma_\phi^{(x)} = 2S_f(0)$ are determined by the low-frequency spectral densities $S_f^{(x)}(\omega)$ of $f_x(t)$, with $x = q, c$.

As explained in sec. 1.1.2, the creation and annihilation operators for the atomic and photonic excitations do not have the same expressions in the dipole and Coulomb gauge (see tab. 1.1):

$$\begin{aligned}
\hat{a}_D &= \hat{\mathcal{U}}^\dagger\hat{a}\hat{\mathcal{U}} = \hat{a} + i\eta\hat{\sigma}_x\,, \\
\sigma_z^C &= \hat{\mathcal{U}}\hat{\sigma}_z\hat{\mathcal{U}}^\dagger = \hat{\sigma}_z\cos\left[2\eta\left(\hat{a}^\dagger + \hat{a}\right)\right] + \hat{\sigma}_y\sin\left[2\eta\left(\hat{a}^\dagger + \hat{a}\right)\right]\,.
\end{aligned} \tag{3.1.10}$$

Thus, these expressions show clearly that (3.1.1) is inadequate. Indeed, following the standard approach, pure dephasing effects can be directly introduced by using Eqs. (3.1.1) and (3.1.5), leading to eq. (3.1.6), but this will lead to incorrect and/or gauge dependent results, because significantly different results will be obtained using $\hat{\mathcal{H}}_s = \hat{\mathcal{H}}_D$ (eq. 1.1.16) or $\hat{\mathcal{H}}_s = \hat{\mathcal{H}}_C$ (eq. 1.1.15) in eq. (3.1.5), especially when the light-matter interaction strength is very strong, as not the Coulomb gauge nor the dipole one can express both photonic and atomic operators in their bare form. As expressed before, light-matter interaction modifies the form of quantum operators describing physical observables, and these changes are gauge dependent [74]. For example, in the Coulomb gauge the form of the physical momentum of the particle is affected by light-matter interaction, while in the dipole gauge, it is interaction independent. On the contrary, the dipole gauge affects the definition of the field momentum. As a consequence, in this gauge, the canonical momentum is no longer proportional to the electric field operator.

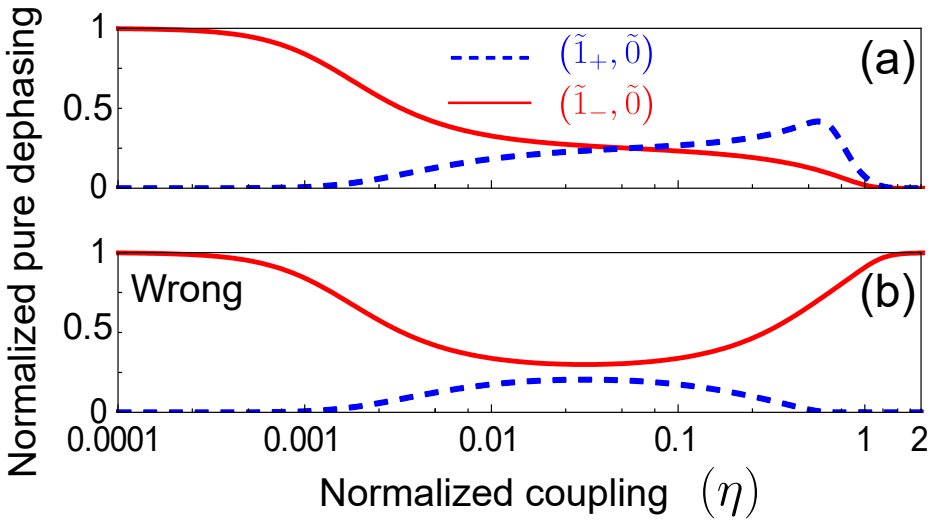

Figure 3.1: Quantum Rabi Model. The normalized pure dephasing rate for the two lowest energy transitions, for a small qubit-cavity detuning $\delta = 3 \times 10^{-3}$ and considering only the qubit pure dephasing. (a) Correct gauge-invariant versus (b) wrong Coulomb gauge results.

We may thus expect that the form of operators describing pure dephasing shall be modified by light-matter interaction too.

In order to obtain correct descriptions of pure dephasing effects, as well as gauge-invariant results, in the presence of light-matter interactions one has to apply the generalized minimal coupling replacements explained in sec. 1.1.2 to pure dephasing perturbations in eq. (3.1.1) too. Applying eqs. (3.1.10) we obtain, in the Coulomb and dipole gauge respectively:

$$\hat{\mathcal{V}}_\phi^C = f_q(t)\hat{\sigma}_z^C + f_c(t)\hat{a}^\dagger\hat{a}\,, \tag{3.1.11}$$

$$\hat{\mathcal{V}}_\phi^D = f_q(t)\hat{\sigma}_z + f_c(t)\hat{a}_D^\dagger\hat{a}_D\,, \tag{3.1.12}$$

These equations allow us to obtain gauge invariant results, restoring, once again, the absolutely arbitrary of choosing a gauge over another.

We will generalize the notation of the JCM to label the QRM states in the following discussion. The ground state will be referred to as $|\tilde{0}\rangle$, while the states that approach the JC states $|n_\pm\rangle$ as the coupling tends to zero will be labelled as $|\tilde{n}_\pm\rangle$. To differentiate between the Coulomb and dipole gauge states, we will use non-primed and primed states, respectively. To illustrate, an analysis of the pure dephasing consequences on the QRM's two lowest transitions, $\alpha_\pm \equiv (\tilde{1}_\pm, \tilde{0})$, will be conducted with a sole focus on qubit pure

dephasing ($f_c(t) = 0$).

After translating to the interaction picture, eq. (3.1.5) yields the following results (see App. C for details):

$$\dot{\tilde{\rho}}_{\alpha'_\pm}(t) = -\left(\gamma_\phi^{\alpha'_\pm}/2\right)\tilde{\rho}_{\alpha'_\pm}(t)\,, \tag{3.1.13}$$

with

$$\gamma_\phi^{\alpha'_\pm} = \frac{\gamma_\phi^{(q)}}{2}\left|\sigma_z^{\tilde{1}'_\pm,\tilde{1}'_\pm} - \sigma_z^{\tilde{0}',\tilde{0}'}\right|^2 . \tag{3.1.14}$$

We observe that the obtained dephasing rates are gauge invariant ($\gamma_\phi^{\alpha'_\pm} = \gamma_\phi^{\alpha_\pm}$), because the expectation values are unitary invariant, when transforming both operators and states: $\gamma_\phi^{\alpha_\pm} = \gamma_\phi^{(q)}|\sigma_z^{C,\tilde{1}_\pm,\tilde{1}_\pm} - \sigma_z^{C,\tilde{0},\tilde{0}}|^2/2$.

Figure 3.1 displays the normalized pure dephasing rate $\gamma_{\tilde{1}'_\pm,\tilde{0}}/\gamma_\phi^0$ for the two lowest energy transitions, considering a small qubit-cavity detuning $\delta = 3\times10^{-3}$ and in the case of only qubit pure dephasing ($\gamma_c = 0$). In the limit of negligible coupling strength, where $|\tilde{1}'_+\rangle \to |e,0\rangle$ and $|\tilde{1}'_-\rangle \to |g,1\rangle$, the standard results are recovered, and only $(\tilde{1}'_-,\tilde{0}')$ is affected by the qubit pure dephasing.

When the detuning and the coupling are comparable, pure dephasing is divided between the two transitions. This is due to the energy eigenstates $|\tilde{1}'_\pm\rangle$ becoming a equally weighted superposition of $|e,0\rangle$ and $|g,1\rangle$. For normalized coupling strengths $\eta > 0.1$ (the USC regime) we start to see discrepancies between the two pictures. For the results obtained with the correct expressions (a), dephasing is less effective for the transition $(\tilde{1}'_-,\tilde{0})$ until both transitions become dephasing-free at stronger couplings (the DSC regime). This phenomenon reflects the fact that a fluctuation at the qubit resonance frequency has a very minor effect on the dressed-state energies when the coupling rate surpasses the bare qubit frequency. Conversely, Fig. 3.1b indicates an incorrect high rate of pure dephasing for the lowest energy transition, showing a maximum in the dephasing rate for the transition $(\tilde{1}'_-,\tilde{0}')$, implying that a zero frequency transition (see the degeneration in Fig. 1.2 impact maximally the dephasing.

3.2 Hopfield model

Another widely used model worth investigating is the Hopfield model [65], also used in Sec. 2.2. Its simplest form describes the interaction of a single-mode electromagnetic resonator with a matter system composed of a collection of fermionic oscillators. The

bosonic matter field creation and annihilation operators are respectively $\hat{b}^\dagger$ and $\hat{b}$. In the dipole gauge the system Hamiltonian is [64]:

$$\hat{H}_{\mathrm{D}} = \hat{H}_0 + i\lambda\,\omega_c(\hat{a}^\dagger - \hat{a})(\hat{b} + \hat{b}^\dagger) + \omega_c\,\lambda^2\,(\hat{b} + \hat{b}^\dagger)^2\,, \tag{3.2.1}$$

where $\hat{H}_0 = \omega_c\hat{a}^\dagger\hat{a} + \omega_x\hat{b}^\dagger\hat{b}$, and λ is the normalized coupling strength. While in the Coulomb gauge is [64]:

$$\hat{H}_C = \hat{H}_0 - i\omega_x\lambda\,(\hat{b}^\dagger - \hat{b})(\hat{a}^\dagger + \hat{a}) + \mathcal{D}(\hat{a}^\dagger + \hat{a})^2\,, \tag{3.2.2}$$

where $\mathcal{D} = \omega_x\lambda^2$. These two Hamiltonians can be directly obtained by generalized minimal coupling replacements: $H_C = \omega_c\hat{a}^\dagger\hat{a} + \omega_x\hat{T}^\dagger\hat{b}^\dagger\hat{b}\hat{T}$ and $H_D = \omega_c\hat{T}\hat{a}^\dagger\hat{a}\hat{T}^\dagger + \omega_x\hat{b}^\dagger\hat{b}$, where $\hat{T} = \exp[-i\lambda(\hat{a} + \hat{a}^\dagger)(\hat{b} + \hat{b}^\dagger)]$, similarly to what is shown in sec. 1.1.2 (note that in this section the unitary transformation is $\hat{T}$, defined as $\hat{U} = \hat{T}^\dagger$ to avoid confusion with the Bogoliubov coefficients that will appear shortly after).

The quasiparticles describing the excitations of this system are called polaritons and the system can be solved by using a Hopfield-Bogoliubov transformation [65]. Since we have two bosonic fields, we will have two polaritons $\hat{P}^\mu$, the lower polariton ($\mu = 1$) and the upper polariton ($\mu = 2$), obtained through a linear combination of $\hat{a}$, $\hat{a}^\dagger$, $\hat{b}$ and $\hat{b}^\dagger$:

$$\hat{P}^\mu = U_b^\mu\hat{b} + U_a^\mu\hat{a} + V_b^\mu\hat{b}^\dagger + V_a^\mu\hat{a}^\dagger\,. \tag{3.2.3}$$

Where we imposed the commutation rules with:

$$|U_b^\mu|^2 + |U_a^\mu|^2 - |V_b^\mu|^2 - |V_a^\mu|^2 = 1\,. \tag{3.2.4}$$

Inverting this equations we obtain:

$$\hat{a} = \sum_{\mu=1}^{2}\left(U_a^\mu P_\mu - V_a^\mu P_\mu^\dagger\right)\,, \tag{3.2.5a}$$

$$\hat{b} = \sum_{\mu=1}^{2}\left(U_b^\mu P_\mu - V_b^\mu P_\mu^\dagger\right)\,. \tag{3.2.5b}$$

This procedure allows us to obtain the polariton eigenfrequencies Ω_μ (which are observable, thus not modified by the gauge choice), and the Hopfield coefficients which are gauge dependent. As a consequence, the polariton operators are gauge dependent.

As said in the previous Sec. 3.1, the expression describing the stochastic fluctuation of the resonance frequencies of the components' dephasing cannot be expressed with

$$\hat{V}_{\mathrm{dep}}(t) = f_c(t)\hat{a}^\dagger\hat{a} + f_x(t)\hat{b}^\dagger\hat{b}\,, \tag{3.2.6}$$

since it will mix operators defined in different gauges. The corrected gauge dependent form is:

$$\hat{V}^D_{\rm dep}(t) = f_c(t)\hat{a}^\dagger_D\hat{a}_D + f_x(t)\hat{b}^\dagger\hat{b}\,, \tag{3.2.7}$$

$$\hat{V}^C_{\rm dep}(t) = f_c(t)\hat{a}^\dagger\hat{a} + f_x(t)\hat{b}^\dagger_C\hat{b}_C\,, \tag{3.2.8}$$

where $\hat{a}_D = \hat{T}\hat{a}\hat{T}^\dagger = \hat{a} + i\lambda(\hat{b}+\hat{b}^\dagger)$ and $\hat{b}_C = \hat{T}^\dagger\hat{b}\hat{T} = \hat{b} - i\lambda(\hat{a}+\hat{a}^\dagger)$. The polariton pure dephasing rates can be obtained by expanding Eqs. (3.2.7) and (3.2.8) in terms of the polariton operators, and then applying the standard master equation method to obtain the Lindbladian terms, in analogy with the results of the previous sec. 3.1. Since the two dephasing contributions are independently from each other, we will treat separately the dephasing on the two bosonic operators to simplify the expressions.

The contribution coming from the matter pure dephasing $\hat{V}^x_{\rm dep} = f_x(t)\hat{b}^\dagger\hat{b}$, in terms of the polariton operators is:

$$\hat{b}^\dagger\hat{b} = A_1\hat{P}^\dagger_1\hat{P}_1 + A_2\hat{P}^\dagger_2\hat{P}_2 + B_{12}\hat{P}^\dagger_1\hat{P}_2 + B_{21}\hat{P}^\dagger_2\hat{P}_1\,, \tag{3.2.9}$$

with

$$A_\mu = |U^\mu_b|^2 + |V^\mu_b|^2\,, \tag{3.2.10}$$

$$B_{12} = B^*_{21} = U^{1\,*}_b U^2_b + V^1_b V^{2\,*}_b\,. \tag{3.2.11}$$

In this expression we discarded the terms that oscillate at high frequency (RWA) and the constants that have no effects on the dynamics. In the interaction picture, this contribution becomes

$$\hat{V}^x_{\rm dep}(t) = f_x(t)\left[A_1\hat{P}^\dagger_1\hat{P}_1 + A_2\hat{P}^\dagger_2\hat{P}_2 + e^{-i\omega_{21}t}B_{12}\hat{P}^\dagger_1\hat{P}_2 + e^{i\omega_{21}t}B_{21}\hat{P}^\dagger_2\hat{P}_1\right]\,, \tag{3.2.12}$$

where $\omega_{21} = \omega_2 - \omega_1$ with the polaritonic eigenfrequencies ω_i. (3.2.12) can be written in a more compact form as

$$\hat{V}^x_{\rm dep} = f_x(t)\left[\hat{D}_{12} + e^{-i\omega_{21}t}\hat{M}_{12} + e^{i\omega_{21}t}\hat{M}^\dagger_{12}\right]\,,$$

with

$$\hat{D}_{12} = A_1\hat{P}^\dagger_1\hat{P}_1 + A_2\hat{P}^\dagger_2\hat{P}_2\,, \tag{3.2.13}$$

$$\hat{M}_{12} = B_{12}\hat{P}^\dagger_1\hat{P}_2\,, \tag{3.2.14}$$

and using the results presented in the previous sections, we obtain

$$\hat{V}^x_{\rm dep}(t) = f_0(t)\hat{D}_{12} + f_{\omega_{21}}(t)\hat{M}_{12} + f_{-\omega_{21}}(t)\hat{M}^\dagger_{12}\,, \tag{3.2.15}$$

with $f_\omega(t)$ expressed in (3.1.4). Thus, the resulting Lindbladian in the case of matter pure dephasing is

$$\mathcal{L}\bullet = \frac{1}{2}\gamma_\phi(\omega_{21})\mathcal{D}[\hat{M}_{12}]\bullet + \frac{1}{2}\gamma_\phi(-\omega_{21})\mathcal{D}[\hat{M}_{12}^\dagger]\bullet + \frac{1}{2}\gamma_\phi(0)\mathcal{D}[\hat{D}_{12}]\bullet\,, \tag{3.2.16}$$

with $\gamma_\phi(\omega) = 2S_f(\omega)$.

The contribution from the cavity pure dephasing in terms of the polariton operators is:

$$\hat{a}^\dagger\hat{a} = A_1\hat{P}_1^\dagger\hat{P}_1 + A_2\hat{P}_2^\dagger\hat{P}_2 + B_{12}\hat{P}_1^\dagger\hat{P}_2 + B_{21}\hat{P}_2^\dagger\hat{P}_1\,, \tag{3.2.17}$$

where

$$A_\mu = |U_a^\mu|^2 + |V_a^\mu|^2\,, \tag{3.2.18}$$

$$B_{12} = B_{21}^* = U_a^{1\,*}U_a^2 + V_a^1V_a^{2\,*}\,. \tag{3.2.19}$$

This yields a Lindbldian of the same form of (3.2.16) with the only difference for the polariton coefficients expressed in Eqs. (3.2.18) and (3.2.19).

As long as we do not consider both these contributions simultaneously, is possible to choose a gauge and obtain correct results. But, as we have seen in sec. 3.1, this approach leads to wrong results if it is not possible to neglect one of them. The use of the Coulomb gauge results in a transformation of the matter operator $\hat{b}$ to $\hat{b}_C = \hat{T}^\dagger\hat{b}\hat{T}$ due to the application of minimal coupling to the matter system. Conversely, the dipole gauge applies minimal coupling to the photonic system, which leads to a *dressed* photonic operator $\hat{a}_D = \hat{T}\hat{a}\hat{T}^\dagger$. This key distinction indicates that the process of polariton diagonalization produces divergent Hopfield coefficients, contingent on whether one chooses the Coulomb or dipole gauge. In particular, in the dipole gauge we have:

$$\hat{b} = \sum_{\mu=1}^{2}\left(U_b^{\mu\prime}P_\mu' - V_b^{\mu\prime}P_\mu'^\dagger\right)\,, \tag{3.2.20}$$

where P_μ' are the polariton operators obtained by diagonalizing the Hopfield Hamiltonian in the dipole gauge. While in the Coulomb gauge we have

$$\begin{aligned}\hat{b}_C &= \hat{T}^\dagger\left[\sum_{\mu=1}^{2}\left(U_b^{\mu\prime}P_\mu' - V_b^{\mu\prime}P_\mu'^\dagger\right)\right]\hat{T}\\ &= \sum_{\mu=1}^{2}\left(U_b^{\mu\prime}\hat{T}^\dagger P_\mu'\hat{T} - V_b^{\mu\prime}\hat{T}^\dagger P_\mu'^\dagger\hat{T}\right)\\ &= \sum_{\mu=1}^{2}\left(U_b^{\mu\prime}P_\mu - V_b^{\mu\prime}P_\mu^\dagger\right)\,,\end{aligned} \tag{3.2.21}$$

which contains the polariton operators obtained by diagonalizing the Hamiltonian in the Coulomb gauge, but with the same coefficients of the dipole gauge. To obtain (3.2.21), we have used the relation

$$P_\mu = \hat{T}^\dagger P'_\mu \hat{T}\,. \tag{3.2.22}$$

To prove this relation we consider the definition of polaritonic operators:

$$[P_\mu, \hat{\mathcal{H}}_C] = \Omega_\mu P_\mu\,, \tag{3.2.23a}$$

$$[P'_\mu, \hat{\mathcal{H}}_D] = \Omega_\mu P'_\mu\,, \tag{3.2.23b}$$

and we can calculate how they transforms from the Coulomb to dipole gauge. Gauge invariance implies that the final result has to be equal to (3.2.23b). We obtain:

$$\begin{aligned}
\hat{T}[P_\mu, \hat{H}_C]\hat{T}^\dagger &= \Omega_\mu \hat{T} P_\mu \hat{T}^\dagger\,, && \text{(3.2.24a)}\\
\hat{T}[P_\mu, \hat{H}_C]\hat{T}^\dagger &= \hat{T}(P_\mu \hat{H}_C - \hat{H}_C P_\mu)\hat{T}^\dagger && \text{(3.2.24b)}\\
&= \hat{T}P_\mu \hat{H}_C \hat{T}^\dagger - \hat{T}\hat{H}_C P_\mu \hat{T}^\dagger\\
&= \hat{T}P_\mu \hat{T}^\dagger \hat{T}\hat{H}_C \hat{T}^\dagger - \hat{T}\hat{H}_C \hat{T}^\dagger \hat{T} P_\mu \hat{T}^\dagger\\
&= \hat{T}P_\mu \hat{T}^\dagger \hat{H}_D - \hat{H}_D \hat{T} P_\mu \hat{T}^\dagger = [\hat{T}P_\mu \hat{T}^\dagger, \hat{H}_D]\,.
\end{aligned}$$

Combining the results of Eqs. (3.2.24a) and (3.2.24b), we obtain:

$$[\hat{T}P_\mu \hat{T}^\dagger, \hat{H}_D] = \Omega_\mu \hat{T} P_\mu \hat{T}^\dagger\,, \tag{3.2.25}$$

which is the definition of the polariton operators P'_μ in the dipole-gauge (which are the operators that allow the diagonalization of $\hat{\mathcal{H}}_D$) given by (3.2.23b). Hence, (3.2.22) is the correct gauge transformation for the polaritonic operators.

The whole analysis described above can be summarized as follows: in the case of matter pure dephasing, the stochastic perturbation is: $\hat{V}^x_{\text{dep}} = f_x(t)\hat{b}^\dagger\hat{b}$ in the dipole gauge, and $\hat{V}^x_{\text{dep}} = f_x(t)\hat{b}^\dagger_C\hat{b}_C$ in the Coulomb gauge, where

$$\hat{b}^\dagger\hat{b} = A'_1\hat{P}'^\dagger_1\hat{P}'_1 + A'_2\hat{P}'^\dagger_2\hat{P}'_2 + B'_{12}\hat{P}'^\dagger_1\hat{P}'_2 + B'_{21}\hat{P}'^\dagger_2\hat{P}'_1\,, \tag{3.2.26}$$

and

$$\hat{b}^\dagger_C\hat{b}_C = A'_1\hat{P}^\dagger_1\hat{P}_1 + A'_2\hat{P}^\dagger_2\hat{P}_2 + B'_{12}\hat{P}^\dagger_1\hat{P}_2 + B'_{21}\hat{P}^\dagger_2\hat{P}_1\,, \tag{3.2.27}$$

with

$$\begin{aligned}
A'_\mu &= \left|U^{\mu\prime}_b\right|^2 + \left|V^{\mu\prime}_b\right|^2\,, && \text{(3.2.28)}\\
B'_{12} &= B'^*_{21} = U^{1\prime *}_b U^{2\prime}_b + V^{1\prime}_b V^{2\prime *}_b\,. && \text{(3.2.29)}
\end{aligned}$$

In order to accurately depict pure dephasing, it is necessary to incorporate the dipole coefficients provided in Eqs. (3.2.28) and (3.2.29) into the Lindbladian formula presented in (3.2.16), despite the use of the Coulomb gauge. Conversely, when dealing with photonic pure dephasing, the stochastic perturbation is represented by $\hat{V}^c_{\text{dep}} = f_c(t)\hat{a}^\dagger\hat{a}$ in the Coulomb gauge, and $\hat{V}^c_{\text{dep}} = f_c(t)\hat{a}^\dagger_D\hat{a}_D$ in the dipole gauge. This means that the Coulomb polariton coefficients must be utilized in the Lindbladian formula even when employing the dipole gauge.

From the obtained master equation, the equations of motion for the mean values of the polariton operators are $\partial_t\langle\hat{P}_\mu\rangle = (-i\Omega_\mu - \gamma^\mu_\phi/2)\langle\hat{P}_\mu\rangle$, where

$$\gamma^\mu_\phi = \gamma^0_c\left(|U^\mu_a|^2 + |V^\mu_a|^2\right) + \gamma^0_x\left(|U^{\mu\,\prime}_b|^2 + |V^{\mu\,\prime}_b|^2\right). \tag{3.2.30}$$

The outcome that can be obtained by disregarding the alterations in the perturbation Hamiltonian induced by the interaction of light and matter, and starting from (3.2.6), can be vastly different from the result obtained through the incorporation of these modifications.

In Fig. 3.2a, we can see the normalized rates of pure dephasing for both polariton modes ($\gamma^\mu_\phi/\gamma^0_x$) in the scenario where there is no photonic noise ($\gamma^0_c = 0$) and considering three distinct values of the detuning between the exciton and cavity (δ). We can observe that, at high coupling rates, the dephasing rate of the lower polariton tends towards zero, regardless of the detuning. This effect is a direct result of the lower polariton's resonance frequency rapidly approaching zero for $\lambda \to \infty$ [refer to Fig. 3.3c], independently of the detuning. This implies that even minor fluctuations in the resonance frequencies of the components do not induce fluctuations or dephasing in the polariton mode.

For comparison, Fig. 3.3ab exhibits an incorrect outcome $\gamma^\mu_\phi/\gamma^0_x = |U^\mu_b|^2 + |V^\mu_b|^2$, which was achieved by ignoring the alterations to the structure of subsystems and observables that may arise due to interaction. This result was obtained for two different detunings, and notable discrepancies become apparent once the system enters the USC regime, with $\lambda \sim 0.1$. Additionally, as the coupling rates become larger and the system enters the DSC regime, the behaviour of the upper and lower polaritons is inverted, leading to further contrasts.

It is important to notice that in a number of experiments, it has been noted that the upper polariton exhibits a greater degree of line broadening compared to the lower

polariton, a discovery which aligns with the outcomes presented in this paper [75, 76, 20, 77]. However, additional research is necessary due to the various broadening mechanisms involved in these systems. The method demonstrated here has the potential to be implemented in more intricate light-matter systems and/or complete quantum models of pure dephasing, as noted in prior works [46, 78].

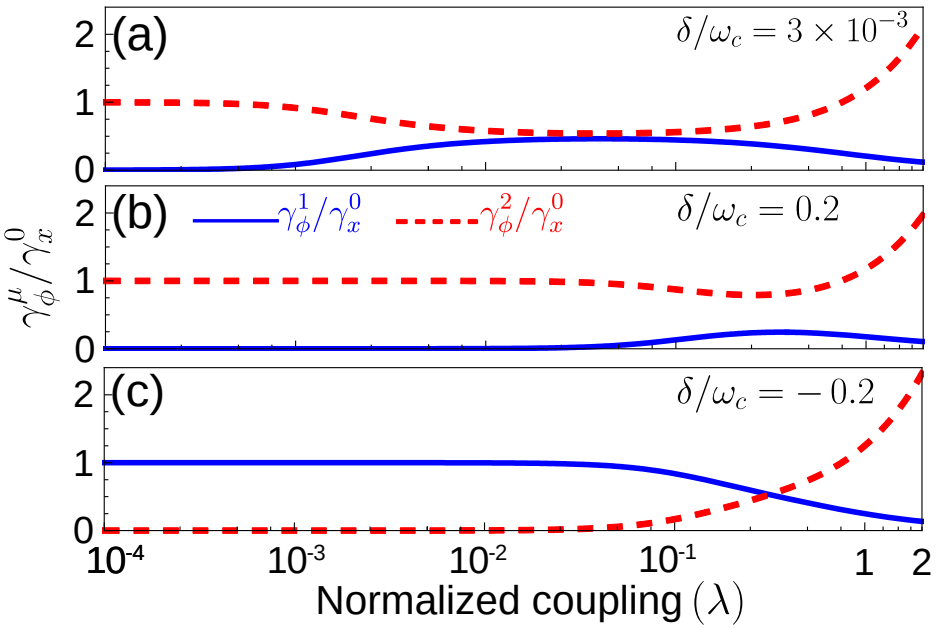

Figure 3.2: Hopfield model. Normalized pure dephasing rate of the lower and upper polaritons, originating from exciton dephasing, versus the normalized coupling strength, obtained for different exciton-cavity detunings, and considering only the matter pure dephasing.

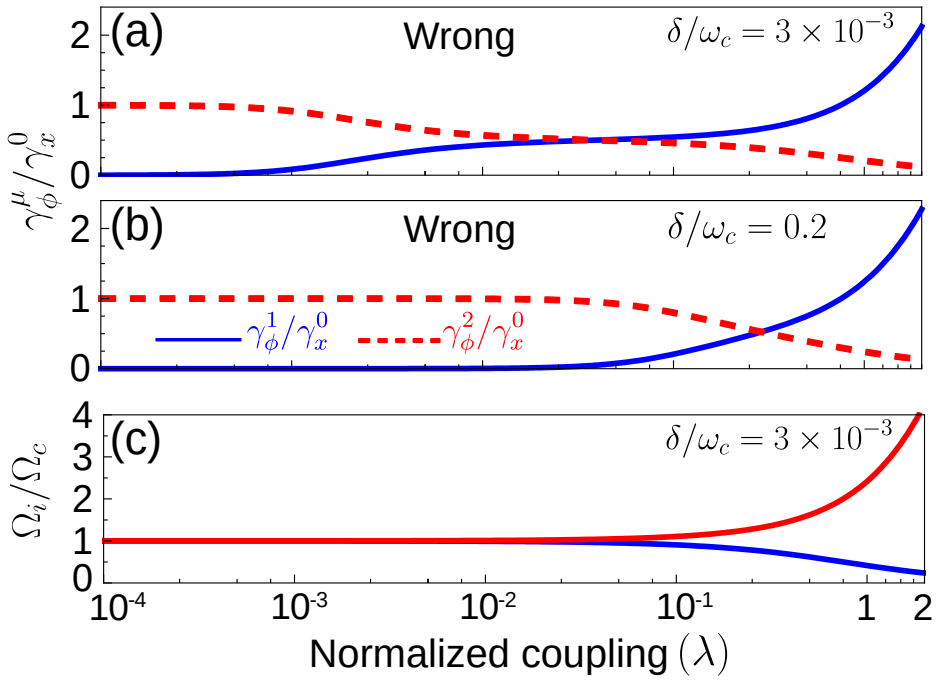

Figure 3.3: Hopfield model. Wrong (see text) normalized pure dephasing rates of the lower and upper polaritons, originating from exciton dephasing, versus the normalized coupling strength, obtained for two different exciton-cavity detunings, and considering only the matter pure dephasing (a, b). Panel (c): frequencies of the two polariton modes for a qubit-cavity detuning $\delta/\omega_c = 3 \times 10^{-3}$.

Chapter 4

Optomechanics

In this chapter we will move our focus to optomechanics, a different hybrid light-matter system and we will show different quantum effects that rise when the coupling is strong enough.

The simplest optomechanical system is a cavity with a movable mirror, but it is still quite complicated to obtain a Hamiltonian description for this system. The challenge of quantizing an electromagnetic field is amplified when the boundary, such as a mirror, is in motion due to radiation pressure. The complexity arises because the movable mirror's boundary condition is contingent upon the field itself. The fluctuation of the field at the quantum level can alter the mirror's position, which subsequently impacts the field. As a result, the most logical approach is to view the mirror and the field as a self-consistent system [79].

Through the use of radiation pressure, it was possible to manipulate quantum mechanical systems, allowing for essential examinations of quantum theory [80, 81], precise measurements [82, 83, 84], and innovative quantum technologies [85, 86, 87]. Laser cooling methods [88, 89, 90] have made it possible to observe quantized vibrational modes of objects on a macroscopic scale and even reach their ground-state [91, 92, 93]. This breakthrough has opened up the potential for the realization of entangled macroscopic states, leading to fresh methods to store and process quantum information [94, 95, 96, 97]. In particular, optomechanical crystals [98, 99, 100] can be scaled to form optomechanical arrays, in which hopping mechanisms can be used to propose applications for quantum information processing [101, 102].

In the following sections, we will introduce the principles of optomechanical coupling

[103] and, after that, our work on two cavities coupled by a movable mirror and its applications. These results are published in [104], and all the figures in this chapter were originally published there.

4.1 Principles of optomechanical coupling

4.1.1 The radiation pressure force and optomechanical coupling

The basic process that links the characteristics of the radiation field within a cavity to the motion of the mechanical system is through the transfer of momentum from photons, which is also known as radiation pressure. The most elementary form of this phenomenon can be considered the transfer of momentum that results from reflection within a Fabry-Perot cavity. A single photon is responsible for transferring momentum of $|\Delta p| = 2h/\lambda$, where λ is the photon wavelength. The radiation pressure force is given by

$$\langle \hat{F} \rangle = 2\hbar k \frac{\langle \hat{a}^\dagger \hat{a} \rangle}{\tau_c} = \hbar \frac{\omega}{L} \langle \hat{a}^\dagger \hat{a} \rangle \,, \tag{4.1.1}$$

where $\tau_c = 2L/c$ is the travel time from one side of the cavity to the other, and $\hbar\dfrac{\omega}{L}$ is the force of radiation pressure produced by one photon. The ratio $G = \omega/L$ describes the change in cavity resonance frequency with position. In the following section, a Hamiltonian explanation of the interaction between an optical cavity and a movable mirror will present this relationship in its complete generality.

In a more broad context, the optomechanical coupling can manifest in various ways. One such way is through the transfer of momentum via reflection, which occurs in systems such as Fabry-Perot cavities with a movable end-mirror or microtoroids. Another method involves coupling through a dispersive shift in the frequency of the cavity, which can be seen in setups that feature a membrane at the centre or levitated nano-objects trapped within the cavity. Finally, the coupling can also be achieved through optical near-field effects, where nano-objects are positioned within the evanescent field of a resonator or a waveguide that is situated just above a substrate.

Regardless of how the force is interpreted physically, the optomechanical interaction that occurs in an optomechanical system can always be deduced by examining the shift in cavity resonance frequency in relation to displacement, which is known as the "dispersive" shift. This will serve as the foundation for our Hamiltonian description, which will be

discussed in the following section.

4.1.2 Hamiltonian formulation

We consider the two uncoupled systems as two harmonic oscillators, the optical part is described by the frequency ω_{cav} and the operators $\hat{a}$ and $\hat{a}^\dagger$, while the mechanical part has frequency Ω_m and operators $\hat{b}$ and $\hat{b}^\dagger$. Thus, the non-interacting Hamiltonian is:

$$\hat{H}_0 = \hbar\omega_{\text{cav}}\hat{a}^\dagger\hat{a} + \hbar\Omega_m\hat{b}^\dagger\hat{b}\,. \tag{4.1.2}$$

Since the movable mirror at one end of the cavity modifies the length of the cavity itself, it has an effect on the optical eigenfrequency. We model it by its series expansion:

$$\omega_{\text{cav}}(x) \approx \omega_{\text{cav}} + x\partial\omega_{\text{cav}}/\partial x + \dots\,. \tag{4.1.3}$$

Usually, stopping the expansion at the linear term is sufficient to describe most of the phenomena appearing in these systems. Calling the optical frequency shift per displacement as $G = -\partial\omega_{\text{cav}}/\partial x$, for a cavity of length L we have $G = \omega_{\text{cav}}/L$. We defined that for $x > 0$ we have an increase in cavity length, leading to a decrease in $\omega_{\text{cav}}(x)$ if $G > 0$. Considering this, the optical Hamiltonian becomes:

$$\hbar\omega_{\text{cav}}(x)\hat{a}^\dagger\hat{a} \approx \hbar(\omega_{\text{cav}} - G\hat{x})\hat{a}^\dagger\hat{a}\,. \tag{4.1.4}$$

Since $\hat{x}$ is the mirror's position, we have $\hat{x} = x_{\text{ZPF}}(\hat{b} + \hat{b}^\dagger)$, where x_{ZPF} is the zero point fluctuation of the mirror. The interaction part of the Hamiltonian, after applying the RWA, can be written as:

$$\hat{H}_{\text{int}} = -\hbar g_0\hat{a}^\dagger\hat{a}(\hat{b} + \hat{b}^\dagger)\,, \tag{4.1.5}$$

where

$$g_0 = Gx_{\text{ZPF}} \tag{4.1.6}$$

is the optomechanical coupling strength expressed as a frequency. Its purpose is to measure the interaction between a single phonon and a single photon. It is important to note that while G depends on the definition of displacement, which can be arbitrary for complex systems, g_0 does not, thus is considered more essential. Another commonly used symbol is g, which is used for the effective optomechanical coupling in the linearized regime. It is amplified compared to g_0 because of the photon field's amplitude. The Hamiltonian indicates that the interaction between a movable mirror and the radiation

field is fundamentally a nonlinear process that involves three operators (three wave mixing).

The radiation pressure force is simply the derivative of $\hat{H}_{\text{int}}$ with respect to displacement:

$$\hat{F} = -\frac{d\hat{H}_{\text{int}}}{d\hat{x}} = \hbar G \hat{a}^\dagger \hat{a} = \hbar \frac{g_0}{x_{\text{ZPF}}} \hat{a}^\dagger \hat{a} \tag{4.1.7}$$

Similarly to the Rabi model, is possible to define a SC regime if $g > \kappa$, where g is the coupling strength defined as $g = g_0\sqrt{\bar{n}_{\text{cav}}}$ and κ are the losses of the system. This definition depends on the number of photons inside the cavity and, thus, on the laser intensity. In order to see nonlinear quantum effects the condition becomes much more stringent, as the single-photon optomechanical coupling rate needs to exceed the cavity decay ($g_0 > \kappa$).

4.2 Extension to two cavities

Moving to a more complex system, in this section we will study two electromagnetic resonators separated by a moving mirror (see Fig. 4.1). This will allow the two cavities to interact through an optomechanical coupling and make photon-pair hopping possible. This particular mechanism has a purely quantum nature since it is also activated in the absence of the field on one side of the cavity (see App. D.1), making it classically impossible. In this case is the presence of virtual particles that fill the quantum vacuum that activates the process.

We obtained the system's Hamiltonian by quantizing the classical problem, generalizing

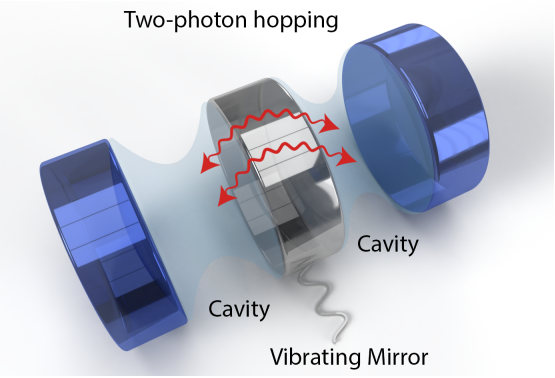

Figure 4.1: Two non-interacting electromagnetic cavities separated by a movable two-sided perfect mirror.

the results in Ref. [79]. While it accounts also for generic equilibrium positions of the mirror, in the following sections we consider only the symmetric case.

Similar models have been explored in previous studies, such as in Ref. [105], where ground state dressing and correlation functions between two distinct regions were analyzed, and in Ref. [106], where dielectric separated the two resonators. Our approach involves second-order effective dynamics, where the two-photon hopping mechanism is a spontaneous coherent process. It is worth noting that the optomechanical hopping described in this study is distinct from photon tunnelling, which is a commonly studied photon hopping mechanism elsewhere [107, 108, 109, 110, 111].

The reason for our interest in these jumping phenomena is the potential for imagining optomechanical lattices and researching their properties concerning thermodynamics and information. As a result, the extended optomechanical lattices would showcase a captivating exchange between the creation of Casimir photon-pairs and the movement of the lattice between sites. Most of the mathematical details of this system can be found in the Appendix. In particular, we present the classical Hamiltonian in App. D.1, how to quantize it in App. D.2, how to apply the generalized James' method to provide an effective resonant explanation in App. D.3 and, briefly the Monte Carlo wave function approach in App. D.4.

In the following sections, we will show both analytical and numerical results for the dissipative system dynamics. In particular, we will present the wave function's evolution over a single quantum trajectory and over an average of 500 quantum trajectories, starting from a Fock state and from a Gaussian coherent pulse.

4.2.1 Quantum Hamiltonian

In this section we present the quantum Hamiltonian of the system. As said before, we consider two non-interacting electromagnetic cavities separated by a vibrating two-sided perfect mirror as sketched in Fig. 4.1. Following Ref. [79] we quantized (see App. D.1 and App. D.2) the classical system obtaining the Hamiltonian ($\hbar = 1$)

$$\begin{aligned}\hat{H} &= \omega_a \hat{a}^\dagger \hat{a} + \omega_b \hat{b}^\dagger \hat{b} + \omega_c \hat{c}^\dagger \hat{c} \\ &+ \frac{g}{2}\left[(\hat{c}+\hat{c}^\dagger)^2 - \left(\frac{\omega_a}{\omega_c}\right)^2 (\hat{a}+\hat{a}^\dagger)^2\right](\hat{b}+\hat{b}^\dagger)\,.\end{aligned} \tag{4.2.1}$$

We denoted as $\hat{b}^\dagger$ and $\hat{b}$ the creation and annihilation operators of the moving mirror,

the creation and annihilation operators of the left cavity are represented as $\hat{a}$ and $\hat{a}^\dagger$, those of the right cavity are represented as $\hat{c}$ and $\hat{c}^\dagger$. ω_a, ω_b, and ω_c are the respective bare energies of the three boson modes. The coupling strength g is defined as $g = \omega_c^2\, x_{\rm zpf}/\pi = \omega_c\, x_{\rm zpf}/(I - q_0)$, where I and q_0 share the same units as $x_{\rm zpf}$ (as explained in D.1). This coupling strength is dependent on both the zero-point-fluctuation amplitude of the mirror ($x_{\rm zpf}$) and the bare energy of a cavity (ω_c), which is taken as the right cavity for convenience. The asymmetrical configurations are considered by the weight ω_a^2/ω_c^2. The linear approximation implicit in (4.2.1) does not lead to instabilities of the ground state, provided that $g\omega_a < \omega_c^2$, or $x_{\rm zpf}\omega_a < \pi$.

At the resonance $\omega_a = \omega_c$ the hopping mechanism is enabled. The scenario we are examining is one in which the mirror's bare frequency is lower than that of the cavity frequency. Fig. 4.2(a) shows a portion of the lowest energy eigenvalues of the full Hamiltonian (4.2.1) (blue dashdotted curves), obtained for a coupling $g = 0.6\omega_b$. Based on the parameters' choice, is possible to identify different sets of avoided levels, each described by its dynamics. In particular, we focussed on the avoided crossing at $\omega_a = \omega_c$ in the black rectangle, and we showed an enlarged view in Fig. 4.2(b). The gap is indicative of the hybridization of the two states $|\psi_1\rangle$ and $|\psi_2\rangle$, which are eigenstates of the full Hamiltonian (4.2.1).

The generalized James' effective approach [112] (see to D.3) allows for the creation of a local effective description represented by red dashed curves, with great accordance with the full Hamiltonian. The obtained Hamiltonian is easier to read and allows us to highlight the different processes that appear. The effective Hamiltonian to the second order is:

$$\begin{aligned}
\hat{H}^{(2)}_{\rm eff} &= \hat{H}^{(2)}_{\rm shift} + \hat{H}^{(2)}_{\rm hop}\,, \\
\hat{H}^{(2)}_{\rm shift} &= \left[\omega_a + \frac{g^2(4\omega_a+\omega_b)}{8\omega_a^2 - 2\omega_b^2}\right](\hat{c}^\dagger\hat{c} + \hat{a}^\dagger\hat{a}) \\
&\quad + \frac{g^2(3\omega_b^2 - 8\omega_a^2)}{(8\omega_a^2 - 2\omega_b^2)\omega_b}\left[(\hat{c}^\dagger\hat{c})^2 + (\hat{a}^\dagger\hat{a})^2\right] \\
&\quad + \left[\omega_b + \frac{4g^2\omega_a}{4\omega_a^2 - \omega_b^2}(\hat{a}^\dagger\hat{a} + \hat{c}^\dagger\hat{c} + \mathbb{1})\right]\hat{b}^\dagger\hat{b} \\
&\quad + \frac{2g^2}{\omega_b}\hat{a}^\dagger\hat{a}\hat{c}^\dagger\hat{c} + \frac{g^2}{2\omega_a - \omega_b}\mathbb{1}\,, \\
\hat{H}^{(2)}_{\rm hop} &= -\frac{g^2\omega_b}{8\omega_a^2 - 2\omega_b^2}(\hat{a}^2\hat{c}^{\dagger 2} + \hat{a}^{\dagger 2}\hat{c}^2)\,.
\end{aligned} \tag{4.2.2}$$

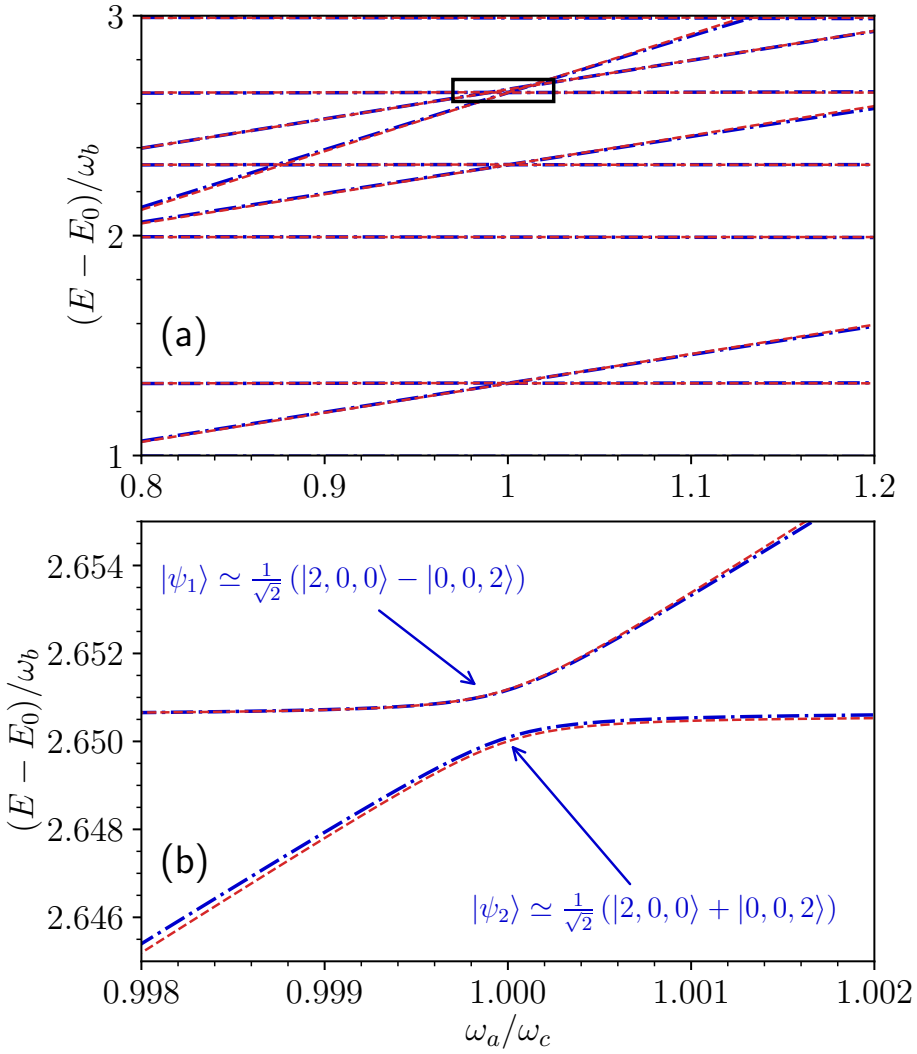

Figure 4.2: (a) The lowest energy levels of the system Hamiltonian versus the ratio between the two cavity frequencies. For a coupling $g = 0.06\,\omega_b$, the position of the avoid level crossing is contained in the black rectangular. (b) An enlarged view of the latter is given. The presence of the labels stresses the hybridization of the two states $|2,0,0\rangle$ and $|0,0,2\rangle$. The frequency mirror was conveniently set as $\omega_b = 3/4\,\omega_c$.

In $\hat{H}^{(2)}_{\text{shift}}$ we grouped all the terms that correspond to only a shift in the system energy. Since $[\hat{a}^\dagger\hat{a}, \hat{H}^{(2)}_{\text{shift}}] = [\hat{b}^\dagger\hat{b}, \hat{H}^{(2)}_{\text{shift}}] = [\hat{c}^\dagger\hat{c}, \hat{H}^{(2)}_{\text{shift}}] = 0$ the unperturbated states $|n_a, n_b, n_c\rangle$, respectively the number of excitations in the left cavity, the mirror and the right cavity, are still a good basis for the system. In $\hat{H}^{(2)}_{\text{hop}}$ are grouped the terms responsible for the two-photon hopping, as these terms destroy two photons in one cavity to create them in the other one.

4.3 Results

4.3.1 Analytical approach

The two states $|\psi_{1,2}\rangle = (|2,0,0\rangle \pm |0,0,2\rangle)/\sqrt{2}$ are eigenstates of the full (effective) Hamiltonian.

For the purpose of a straightforward analysis, we limit our examination to the subspace spanned by $\{|2,0,0\rangle, |0,0,2\rangle\}$, specifically in the vicinity of the avoided-level crossing. When the system is initialized in either $|2,0,0\rangle$ or $|0,0,2\rangle$, we can observe a coherent and oscillatory behaviour between the two states of photon-pair that are maximally entangled. The effective interaction Hamiltonian $\hat{H}^{(2)}_{\text{hop}}$ in equation (4.2.2) can be applied to solve the stochastic development of the system wave function by disregarding any dressing energy shifts that have been absorbed by selecting the appropriate coefficients (refer to App. D.4 for more information). By projecting the time-evolution operator $\hat{U}(t) = \exp\left(-i\hat{\mathcal{H}}t\right)$ onto the $2D$ subspace $\{|2,0,0\rangle, |0,0,2\rangle\}$, with

$$\hat{\mathcal{H}} = \hat{H}^{(2)}_{\text{hop}} - i(\gamma_a\hat{a}^\dagger\hat{a} + \gamma_b\hat{b}^\dagger\hat{b} + \gamma_c\hat{c}^\dagger\hat{c})/2\,, \tag{4.3.1}$$

in the interaction picture we obtain

$$\begin{aligned}\hat{U}(t) \;=\; & e^{-2\gamma t}\left[\cos(\tilde{g}t)\left(|2,0,0\rangle\langle 2,0,0| + |0,0,2\rangle\langle 0,0,2|\right)\right.\\ & \left. - i\sin(\tilde{g}t)\left(|2,0,0\rangle\langle 0,0,2| + |0,0,2\rangle\langle 2,0,0|\right)\right]\,,\end{aligned} \tag{4.3.2}$$

where we choose $\gamma = \gamma_a = \gamma_c$ and $\tilde{g} = g^2\omega_b/2(4\omega_a^2 - \omega_b^2)$. If we initialize the system in the state $|2,0,0\rangle$, its evolution at time t, before a quantum jump takes place, is

$$|\psi(t)\rangle = e^{-2\gamma t}\left[\cos(\tilde{g}t)\,|2,0,0\rangle - i\sin(\tilde{g}t)\,|0,0,2\rangle\right]\,. \tag{4.3.3}$$

By appropriately renormalizing the wave function, we obtain the mean photon number for the left and right cavities and for the mechanical resonator

$$\begin{aligned} \langle \hat{a}^\dagger \hat{a} \rangle &= 2\cos^2(\tilde{g}t)\,, \\ \langle \hat{b}^\dagger \hat{b} \rangle &= 0\,, \\ \langle \hat{c}^\dagger \hat{c} \rangle &= 2\sin^2(\tilde{g}t)\,. \end{aligned} \tag{4.3.4}$$

4.3.2 Numerical approach - Initial Fock state

We will now analyze numerical simulations obtained using eq. (4.3.4). In Fig. 4.3 (a) we see the expectation values on a single quantum trajectory, obtained by solving the stochastic evolution of the system wave function. We initialized the system in $|2,0,0\rangle$, while the parameters are $g = 0.06\,\omega_b$, $\omega_a = \omega_c = 4\omega_b/3$, and $\gamma_a = \gamma_b = \gamma_c = \gamma = 10^{-4}\omega_b$. As above, a refers to the left cavity (blue line), b refers to the mirror (red dashed line) and c refers to the right cavity (black dashed-dotted line). Since this is a single trajectory, we see a coherent hopping of a photon pair from one cavity to the other while the mirror remains in its ground state, as predicted in (4.3.4). When one of the two cavities emits a photon, in this case the one on the right, the photon number inside the cavity that has emitted jumps to one (in this case corresponding to the state $-i\,|0,0,1\rangle = \hat{c}\,|\psi(t)\rangle\,/[\langle\psi(t)|\,\hat{c}^\dagger\hat{c}\,|\psi(t)\rangle]^{1/2}$), while the other jumps to zero, showing the collapse of wave function after a measurement. This excitation is trapped in the cavity until another emission process because the Hamiltonian (4.3.4) does not permit the tunnelling of a single photon from one cavity to the other.

Fig. 4.3 (b) shows the averaged quantities over 500 trajectories (ideally the average should be over infinite trajectories). We clearly see a coherent oscillation of photon-pair. This result, if averaged over a sufficient number of trajectories, is equivalent to the one obtained through a master equation approach, but it lacks the trapping effect after an emission that is possible to see only applying a post-selection procedure [113, 114].

Note that, with the parameters used we obtain an effective coupling $\tilde{g} \approx 3 \times 10^{-4}\omega_b$, which is almost three times greater than the loss rate γ (the latter related to the cavity quality factor Q). This regime, defined as strong coupling, allows the photon pairs to flow from one cavity to the other for a certain time before one photon is lost to the

environment.

4.3.3 Numerical approach - Gaussian coherent pulse drive

Finally, we consider the case of an incoming Gaussian coherent pulse driving the left cavity while the system is initially in its ground state. For simplicity, we present a numerical simulation for the closed dynamics. Figure 4.4 shows the first matrix elements of the density operator at the end of the dynamics. The state of the right cavity contains only even occupation numbers: in a closed dynamics no loss is possible and the hopping mechanism always involves photon pairs.

The phenomena discussed in this paper could be verified experimentally by employing circuit-optomechanical systems, with the chosen parameters. These systems would require either ultra-high-frequency mechanical micro- or nano-resonators operating in the GHz spectral range, or two LC circuits coupled by a SQUID. Furthermore, the optomechanical system proposed in this paper would enable the investigation of a novel mechanism of photon-pair propagation in optomechanical lattices [115, 116], by utilizing arrays of cavities that exhibit non-linear interactions and photon blockade [117]. This would result in the formation of a photon crystal with a periodic modulation.

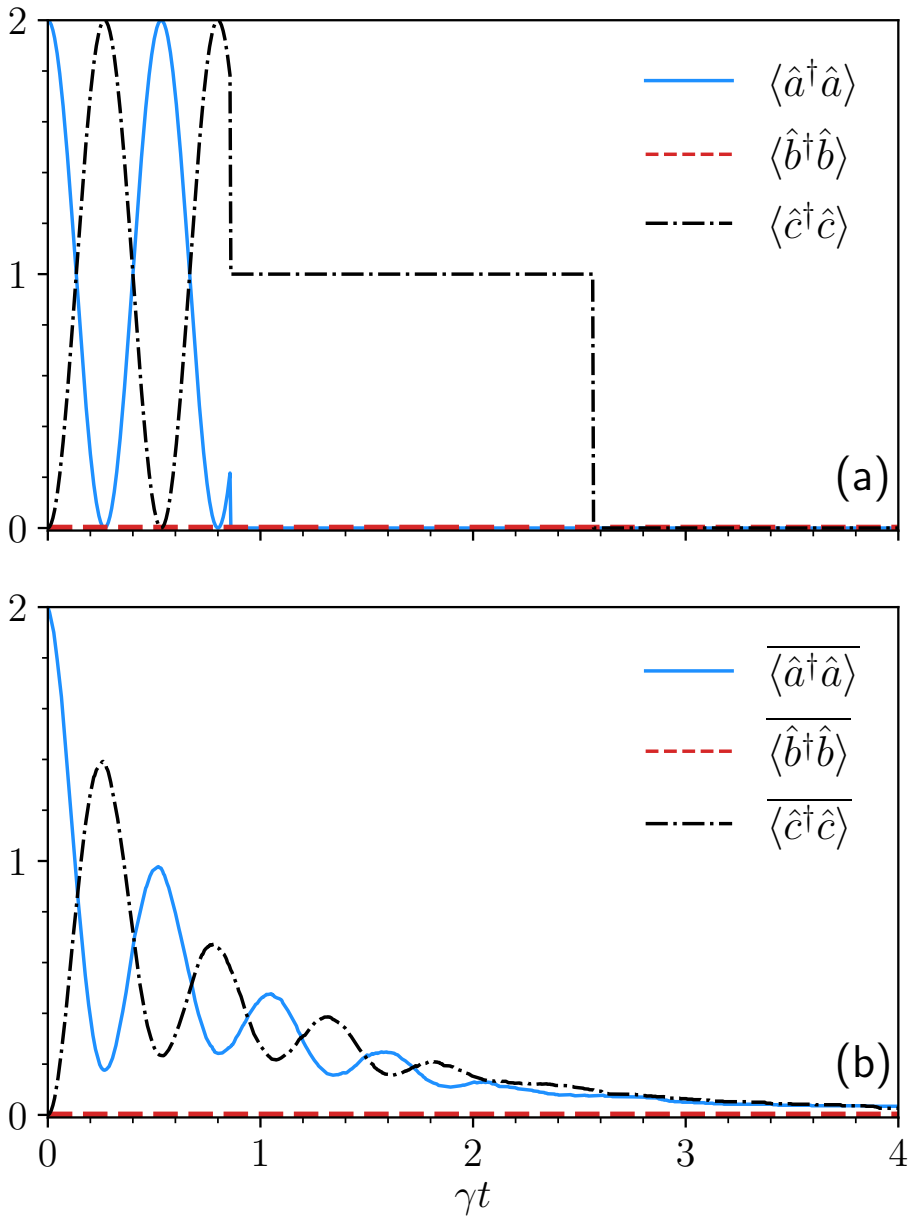

Figure 4.3: The figure shows the quantum dynamics of two cavities and a mirror. Panel (a) is a single quantum trajectory, where the system starts with two photons in the left cavity and none in the right cavity or the mirror. The photon number in each subsystem oscillates until a quantum jump happens in the right cavity, which traps the photon there. After another jump, the system ends up with no photons nor phonons. Panel (b) is an average of 500 trajectories, which shows a coherent evolution of photon pairs. This can also be obtained by a master equation, but it does not capture the trapping effect. The parameters are $g = 0.06\,\omega_b$, $\omega_a = \omega_c = 4\omega_b/3$, and $\gamma_a = \gamma_b = \gamma_c = \gamma = 10^{-4}\omega_b$.

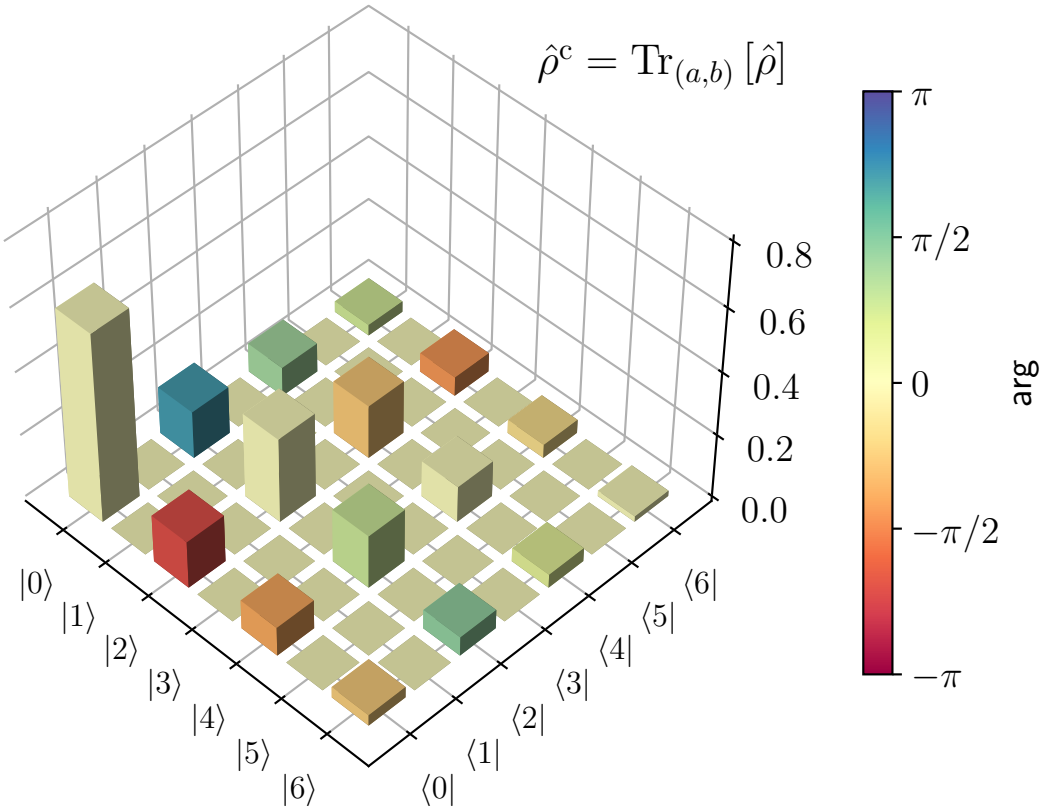

Figure 4.4: Density matrix elements for the right cavity obtained by tracing out the left cavity and the mirror. When the right cavity starts empty and a coherent pulse enters the left cavity, only the states with an even number of photons are populated. This confirms our proposed mechanism of photon hopping. We used the following parameters: $g = 0.09\,\omega_b$, $\omega_a = \omega_c = 1.1\omega_b$, and $\gamma_a = \gamma_b = \gamma_c = 0$.

Chapter 5

Conclusions and outlooks

In this thesis I analyzed multiple hybrid quantum systems in the USC regime. In the first chapter, I showed the state of the art, introducing the Quantum Rabi model and the peculiar effects that arise when the light-matter coupling enters the USC regime. I discussed the presence of virtual photons in the ground state and the apparent violation of the gauge invariance, the principal theoretical problems that emerged in this regime, and showed how to solve these issues.

In the second chapter, I analyzed the gauge issues of a generalized QRM, obtained by considering a non-linear cavity interacting with a two-level atom. I provided a polaritonic model to obtain the correct Hamiltonian for the non-linear interaction and used it to show how important it is to correctly apply the minimal coupling procedure to obtain consistent results that avoid unphysical effects. Differently from the usual QRM, I have found that also the standard dipole-gauge interaction violates the gauge principle, and provides wrong results, in the present case of a nonlinear optical resonator. I also showed how the standard Kerr model becomes questionable for strong coupling rates, comparable with the frequency of the atom and how it depends on the normalized coefficient J of the photonic nonlinearity, on the qubit-oscillator normalized coupling strength η, and on the considered energy levels.

In the third chapter, I demonstrated a correct method for computing the pure dephasing rate through the examination of two representative models of cavity QED systems: the QRM and the Hopfield model. Our findings indicate a decrease in the impact of pure dephasing on the lower polariton branch in the USC regime within the latter model, with further coupling serving to additionally suppress this effect. Conversely, an increase

in pure dephasing is observed in the upper polariton branch with increases in coupling strength. The primary takeaway is that when the rate of light-matter interaction reaches a level comparable to the bare resonance frequencies of the relevant transitions of the system components, the generalized minimal coupling replacements that introduce the light-matter interaction must be applied to any perturbation that affects the matter or light subsystems.

In the fourth chapter, our analysis has delved into the theoretical aspects of an optomechanical system composed of two electromagnetic resonators separated by a vibrating mirror. The Hamiltonian for this system is obtained through canonical quantization and also considers the mirror's generic equilibrium positions. The most significant outcome of our analysis is the revelation of a mechanism where photon pairs can hop in a coherent second-order effective resonant dynamics. The generalized James' approach has been employed to provide analytical insight into this specific phenomenon. Upon conducting a numerical analysis of the energy levels with the lowest values, an avoided-level crossing was observed in proximity to the resonant condition. This gap is indicative of the hybridization of two photon-pair states. By conducting a stochastic evolution of the system's wave function, it was possible to observe coherent oscillatory dynamics between the $|2,0,0\rangle$ and $|0,0,2\rangle$ states.

About the possible expansion of the results presented in this thesis, an immediate expansion of the work presented in the second chapter would be to include system losses and study its dynamics, finding a threshold on both the nonlinearity and the coupling strength that allows us to see experimentally the results obtained.

A future objective is to apply and expand the work presented in this thesis to superconducting circuits. USC has been achieved in many setups, but the environmental noise needed to see the coherent effects characterizing USC has to be low enough that very low temperatures have to be involved (in the order of the tenth-hundreds of mK). Adding this to the recent advancements in experimental techniques that allowed different types of superconducting qubits to reach the USC regime, attracted much focus to this topic. Additionally, superconducting systems have also been used to simulate optomechanical systems. To this end, the results presented in chapter three would also be very important, since losses and dephasing are major issues to build a quantum computer.

Another focal point would be expanding the study of the USC regime in optomechanics.

Considering the system presented in the fourth chapter, it would be interesting to see how the system behaves if the two cavities have different sizes. Additionally, considering an array of cavities coupled in the USC regime by oscillating mirrors might be an interesting platform to study new and maybe surprising thermodynamical effects.

I believe that with minimal adjustments it is possible to apply the various results of this thesis to superconducting circuits and observe them experimentally soon.

Bibliography

[1] E. M. Purcell. “Spontaneous emission probabilities at radio frequencies”. In: *Phys. Rev.* 69 (1946), p. 681.

[2] Wen-Hao Chang et al. “Efficient single-photon sources based on low-density quantum dots in photonic-crystal nanocavities”. In: *Physical review letters* 96.11 (2006), p. 117401.

[3] Y Kaluzny et al. “Observation of self-induced Rabi oscillations in two-level atoms excited inside a resonant cavity: The ringing regime of superradiance”. In: *Physical review letters* 51.13 (1983), p. 1175.

[4] Kerry J Vahala. “Optical microcavities”. In: *nature* 424.6950 (2003), pp. 839–846.

[5] Andrew J Shields. “Semiconductor quantum light sources”. In: *Nature photonics* 1.4 (2007), pp. 215–223.

[6] CL Salter et al. “An entangled-light-emitting diode”. In: *Nature* 465.7298 (2010), pp. 594–597.

[7] Serge Haroche. “Nobel Lecture: Controlling photons in a box and exploring the quantum to classical boundary”. In: *Reviews of Modern Physics* 85.3 (2013), p. 1083.

[8] Iulia Georgescu and Franco Nori. “Quantum technologies: an old new story”. In: *Physics World* 25.05 (2012), p. 16.

[9] P Cappellaro, CL Degen, and F Reinhard. “Quantum sensing”. In: *Rev. Mod. Phys* 89 (2017), p. 035002.

[10] Göran Wendin. “Quantum information processing with superconducting circuits: a review”. In: *Reports on Progress in Physics* 80.10 (2017), p. 106001.

[11] Cristiano Ciuti, Gérald Bastard, and Iacopo Carusotto. "Quantum vacuum properties of the intersubband cavity polariton field". In: *Physical Review B* 72.11 (2005), p. 115303.

[12] Aji A Anappara et al. "Signatures of the ultrastrong light-matter coupling regime". In: *Physical Review B* 79.20 (2009), p. 201303.

[13] Benjamin Askenazi et al. "Midinfrared ultrastrong light–matter coupling for THz thermal emission". In: *ACS photonics* 4.10 (2017), pp. 2550–2555.

[14] Markus Geiser et al. "Ultrastrong coupling regime and plasmon polaritons in parabolic semiconductor quantum wells". In: *Physical Review Letters* 108.10 (2012), p. 106402.

[15] Thomas Niemczyk et al. "Circuit quantum electrodynamics in the ultrastrong-coupling regime". In: *Nature Physics* 6.10 (2010), pp. 772–776.

[16] Fumiki Yoshihara et al. "Superconducting qubit–oscillator circuit beyond the ultrastrong-coupling regime". In: *Nature Physics* 13.1 (2017), pp. 44–47.

[17] Fumiki Yoshihara et al. "Inversion of qubit energy levels in qubit-oscillator circuits in the deep-strong-coupling regime". In: *Physical review letters* 120.18 (2018), p. 183601.

[18] Curdin Maissen et al. "Ultrastrong coupling in the near field of complementary split-ring resonators". In: *Physical Review B* 90.20 (2014), p. 205309.

[19] Janine Keller et al. "Critical softening of cavity cyclotron polariton modes in strained germanium 2D hole gas in the ultra-strong coupling regime". In: *arXiv preprint arXiv:1708.07773* (2017).

[20] Andreas Bayer et al. "Terahertz light–matter interaction beyond unity coupling strength". In: *Nano letters* 17.10 (2017), pp. 6340–6344.

[21] Armando Genco et al. "Bright Polariton Coumarin-Based OLEDs Operating in the Ultrastrong Coupling Regime". In: *Advanced Optical Materials* 6.17 (2018), p. 1800364.

[22] Fábio Barachati et al. "Tunable third-harmonic generation from polaritons in the ultrastrong coupling regime". In: *Acs Photonics* 5.1 (2018), pp. 119–125.

[23] Elad Eizner et al. "Organic photodiodes with an extended responsivity using ultrastrong light–matter coupling". In: *ACS Photonics* 5.7 (2018), pp. 2921–2927.

[24] Felix Benz et al. “Single-molecule optomechanics in “picocavities””. In: *Science* 354.6313 (2016), pp. 726–729.

[25] Jino George et al. “Multiple Rabi splittings under ultrastrong vibrational coupling”. In: *Physical review letters* 117.15 (2016), p. 153601.

[26] Anton Frisk Kockum et al. “Ultrastrong coupling between light and matter”. In: *Nature Reviews Physics* 1.1 (2019), pp. 19–40.

[27] P Forn-Díaz et al. “Ultrastrong coupling regimes of light-matter interaction”. In: *Reviews of Modern Physics* 91.2 (2019), p. 025005.

[28] Daniele De Bernardis et al. “Breakdown of gauge invariance in ultrastrong-coupling cavity QED”. In: *Physical Review A* 98.5 (2018), p. 053819.

[29] Zongping Gong, Ryusuke Hamazaki, and Masahito Ueda. “Discrete time-crystalline order in cavity and circuit QED systems”. In: *Physical review letters* 120.4 (2018), p. 040404.

[30] I. I. Rabi. “On the process of space quantization”. In: *Physical Review* 49.4 (1936), p. 324.

[31] I. I. Rabi. “Space quantization in a gyrating magnetic field”. In: *Physical Review* 51.8 (1937), p. 652.

[32] Serge Haroche and J-M Raimond. *Exploring the quantum: atoms, cavities, and photons*. Oxford university press, 2006.

[33] Cristiano Ciuti and Iacopo Carusotto. “Input-output theory of cavities in the ultrastrong coupling regime: The case of time-independent cavity parameters”. In: *Physical Review A* 74.3 (2006), p. 033811.

[34] Alessandro Ridolfo et al. “Photon blockade in the ultrastrong coupling regime”. In: *Physical review letters* 109.19 (2012), p. 193602.

[35] Omar Di Stefano et al. “Resolution of gauge ambiguities in ultrastrong-coupling cavity quantum electrodynamics”. In: *Nature Physics* 15.8 (2019), pp. 803–808.

[36] L Amico et al. “Integrable spin–boson models descending from rational six-vertex models”. In: *Nuclear Physics B* 787.3 (2007), pp. 283–300.

[37] Daniel Braak. “Integrability of the Rabi model”. In: *Physical Review Letters* 107.10 (2011), p. 100401.

[38] S Ashhab. "Attempt to find the hidden symmetry in the asymmetric quantum Rabi model". In: *Physical Review A* 101.2 (2020), p. 023808.

[39] Anton Frisk Kockum et al. "Deterministic quantum nonlinear optics with single atoms and virtual photons". In: *Physical Review A* 95.6 (2017), p. 063849.

[40] Roy J Glauber. "The quantum theory of optical coherence". In: *Physical Review* 130.6 (1963), p. 2529.

[41] DF Walls. *GJ Milburn, Quantum Optics (Springer, Berlin.* 1994.

[42] Omar Di Stefano et al. "Photodetection probability in quantum systems with arbitrarily strong light-matter interaction". In: *Scientific Reports* 8.1 (2018), p. 17825.

[43] Jared Lolli et al. "Ancillary qubit spectroscopy of vacua in cavity and circuit quantum electrodynamics". In: *Physical review letters* 114.18 (2015), p. 183601.

[44] Mauro Cirio et al. "Amplified optomechanical transduction of virtual radiation pressure". In: *Physical review letters* 119.5 (2017), p. 053601.

[45] Simone De Liberato, Cristiano Ciuti, and Iacopo Carusotto. "Quantum vacuum radiation spectra from a semiconductor microcavity with a time-modulated vacuum Rabi frequency". In: *Physical review letters* 98.10 (2007), p. 103602.

[46] Félix Beaudoin, Jay M Gambetta, and A Blais. "Dissipation and ultrastrong coupling in circuit QED". In: *Physical Review A* 84.4 (2011), p. 043832.

[47] K Takashima et al. "Nonstationary boundary effect for a quantum flux in superconducting nanocircuits". In: *Journal of Physics A: Mathematical and Theoretical* 41.16 (2008), p. 164036.

[48] Iacopo Carusotto et al. "Back-reaction effects of quantum vacuum in cavity quantum electrodynamics". In: *Physical Review A* 85.2 (2012), p. 023805.

[49] L Garziano et al. "Switching on and off of ultrastrong light-matter interaction: Photon statistics of quantum vacuum radiation". In: *Physical Review A* 88.6 (2013), p. 063829.

[50] G Günter et al. "Sub-cycle switch-on of ultrastrong light-matter interaction". In: *Nature* 458.7235 (2009), pp. 178–181.

[51] Alessandro Ridolfo et al. "All optical switch of vacuum Rabi oscillations: The ultrafast quantum eraser". In: *Physical Review Letters* 106.1 (2011), p. 013601.

[52] Jin-Feng Huang, CK Law, et al. "Photon emission via vacuum-dressed intermediate states under ultrastrong coupling". In: *Physical Review A* 89.3 (2014), p. 033827.

[53] Simone De Liberato. "Virtual photons in the ground state of a dissipative system". In: *Nature communications* 8.1 (2017), p. 1465.

[54] Christopher M Wilson et al. "Observation of the dynamical Casimir effect in a superconducting circuit". In: *nature* 479.7373 (2011), pp. 376–379.

[55] Vincenzo Macrì et al. "Nonperturbative dynamical Casimir effect in optomechanical systems: vacuum Casimir-rabi splittings". In: *Physical Review X* 8.1 (2018), p. 011031.

[56] M Babiker and Rodney Loudon. "Derivation of the Power-Zienau-Woolley Hamiltonian in quantum electrodynamics by gauge transformation". In: *Proceedings of the Royal Society of London. A. Mathematical and Physical Sciences* 385.1789 (1983), pp. 439–460.

[57] Anthony F Starace. "Length and velocity formulas in approximate oscillator-strength calculations". In: *Physical Review A* 3.4 (1971), p. 1242.

[58] R Girlanda, A Quattropani, and P Schwendimann. "Two-photon transitions to exciton states in semiconductors. Application to CuCl". In: *Physical Review B* 24.4 (1981), p. 2009.

[59] Sohrab Ismail-Beigi, Eric K Chang, and Steven G Louie. "Coupling of nonlocal potentials to electromagnetic fields". In: *Physical Review Letters* 87.8 (2001), p. 087402.

[60] O. Di Stefano et al. "Resolution of gauge ambiguities in ultrastrong-coupling cavity quantum electrodynamics". In: *Nature Phys.* 15 (2019), p. 803. ISSN: 1745-2473.

[61] Alessio Settineri et al. "Gauge freedom, quantum measurements, and time-dependent interactions in cavity QED". In: *Phys. Rev. Research* 3 (2 2021), p. 023079.

[62] Juan Jose Garcia-Ripoll, Borja Peropadre, and Simone De Liberato. "Light-matter decoupling and A 2 term detection in superconducting circuits". In: *Scientific reports* 5.1 (2015), p. 16055.

[63] Fabio Mauceri et al. “Ultrastrong coupling of a qubit with a nonlinear optical resonator”. In: *Physical Review A* 105.2 (2022), p. 023719.

[64] Luigi Garziano et al. “Gauge invariance of the Dicke and Hopfield models”. In: *Phys. Rev. A* 102.2 (2020), p. 023718.

[65] J. J. Hopfield. “Theory of the Contribution of Excitons to the Complex Dielectric Constant of Crystals”. In: *Phys. Rev.* 112 (5 1958), pp. 1555–1567.

[66] S Savasta and R Girlanda. “Quantum description of the input and output electromagnetic fields in a polarizable confined system”. In: *Phys. Rev. A* 53.4 (1996), p. 2716.

[67] T. Yu and J. H. Eberly. “Qubit disentanglement and decoherence via dephasing”. In: *Phys. Rev. B* 68 (16 2003), p. 165322.

[68] Wojciech Hubert Zurek. “Decoherence, einselection, and the quantum origins of the classical”. In: *Rev. Mod. Phys.* 75 (3 2003), pp. 715–775.

[69] S. Habib, K. Shizume, and W. H. Zurek. “Decoherence, chaos, and the correspondence principle”. In: *Phys. Rev. Lett.* 80.20 (1998), p. 4361.

[70] Alexia Auffèves et al. “Controlling the dynamics of a coupled atom-cavity system by pure dephasing”. In: *Phys. Rev. B* 81 (24 2010), p. 245419.

[71] Alberto Mercurio et al. “Pure Dephasing of Light-Matter Systems in the Ultrastrong and Deep-Strong Coupling Regimes”. In: *Physical Review Letters* 130.12 (2023), p. 123601.

[72] A. Settineri et al. “Dissipation and thermal noise in hybrid quantum systems in the ultrastrong-coupling regime”. In: *Phys. Rev. A* 98 (2018), p. 053834.

[73] H.-P. Breuer and F. Petruccione. *The Theory of Open Quantum Systems*. Oxford University Press, 2002. ISBN: 0-19-852063-8.

[74] C. Cohen-Tannoudji, J. Dupont-Roc, and G. Grynberg. *Photons and Atoms-Introduction to Quantum Electrodynamics*. Wiley-VCH,New York, 1997.

[75] G. Scalari et al. “Ultrastrong Coupling of the Cyclotron Transition of a 2D Electron Gas to a THz Metamaterial”. In: *Science* 335 (2012), p. 1323.

[76] S. Gambino et al. “Exploring Light–Matter Interaction Phenomena under Ultrastrong Coupling Regime”. In: *ACS Photonics* 1 (2014), p. 1042.

[77] S. Rajabali et al. “The Upper Branch Broadening in Ultrastrongly Coupled THz Landau Polaritons”. In: *2019 44th International Conference on Infrared, Millimeter, and Terahertz Waves (IRMMW-THz)*. 2019, p. 1.

[78] H. Carmichael. *An open systems approach to quantum optics*. Vol. 18. Springer Science & Business Media, 2009.

[79] C. K. Law. “Interaction between a moving mirror and radiation pressure: A Hamiltonian formulation”. In: *Phys. Rev. A* 51 (3 1995), pp. 2537–2541.

[80] W. Marshall et al. “Towards Quantum Superpositions of a Mirror”. In: *Phys. Rev. Lett.* 91 (13 2003), p. 130401.

[81] E. Gavartin, P. Verlot, and T. J. Kippenberg. “A hybrid on-chip optomechanical transducer for ultrasensitive force measurements”. In: *Nature Nanotechnology* 7.8 (2012), pp. 509–514. ISSN: 1748-3395.

[82] J. D. Teufel et al. “Nanomechanical motion measured with an imprecision below that at the standard quantum limit”. In: *Nature Nanotechnology* 4.12 (2009), pp. 820–823. ISSN: 1748-3395.

[83] Alexander G. Krause et al. “A high-resolution microchip optomechanical accelerometer”. In: *Nature Photonics* 6.11 (2012), pp. 768–772. ISSN: 1749-4893.

[84] Matteo Carlesso and Mauro Paternostro. “Opto-Mechanical Test of Collapse Models”. In: *Do Wave Functions Jump? : Perspectives of the Work of GianCarlo Ghirardi*. Ed. by Valia Allori et al. Cham: Springer International Publishing, 2021, pp. 205–215. ISBN: 978-3-030-46777-7.

[85] G. Anetsberger et al. “Near-field cavity optomechanics with nanomechanical oscillators”. In: *Nature Physics* 5.12 (2009), pp. 909–914. ISSN: 1745-2481.

[86] P. Verlot et al. “Scheme to Probe Optomechanical Correlations between Two Optical Beams Down to the Quantum Level”. In: *Phys. Rev. Lett.* 102 (10 2009), p. 103601.

[87] Shabir Barzanjeh et al. “Optomechanics for quantum technologies”. In: *Nature Physics* 18.1 (2022), pp. 15–24. ISSN: 1745-2481.

[88] A. Schliesser et al. “Resolved-sideband cooling and position measurement of a micromechanical oscillator close to the Heisenberg uncertainty limit”. In: *Nature Physics* 5.7 (2009), pp. 509–514. ISSN: 1745-2481.

[89] Simon Gröblacher et al. “Demonstration of an ultracold micro-optomechanical oscillator in a cryogenic cavity”. In: *Nature Physics* 5.7 (2009), pp. 485–488. ISSN: 1745-2481.

[90] J. D. Teufel et al. “Sideband cooling of micromechanical motion to the quantum ground state”. In: *Nature* 475.7356 (2011), pp. 359–363. ISSN: 1476-4687.

[91] I. Wilson-Rae et al. “Theory of Ground State Cooling of a Mechanical Oscillator Using Dynamical Backaction”. In: *Phys. Rev. Lett.* 99 (9 2007), p. 093901.

[92] Jasper Chan et al. “Laser cooling of a nanomechanical oscillator into its quantum ground state”. In: *Nature* 478.7367 (2011), pp. 89–92. ISSN: 1476-4687.

[93] T. Ojanen and K. Børkje. “Ground-state cooling of mechanical motion in the unresolved sideband regime by use of optomechanically induced transparency”. In: *Phys. Rev. A* 90 (1 2014), p. 013824.

[94] K. Stannigel et al. “Optomechanical Quantum Information Processing with Photons and Phonons”. In: *Phys. Rev. Lett.* 109 (1 2012), p. 013603.

[95] L. Garziano et al. “Single-step arbitrary control of mechanical quantum states in ultrastrong optomechanics”. In: *Phys. Rev. A* 91 (2 2015), p. 023809.

[96] P. Meystre. “A short walk through quantum optomechanics”. In: *Annalen der Physik* 525.3 (2013), pp. 215–233.

[97] V. Macrí et al. “Deterministic synthesis of mechanical NOON states in ultrastrong optomechanics”. In: *Phys. Rev. A* 94 (1 2016), p. 013817.

[98] M. Eichenfield et al. “A picogram- and nanometre-scale photonic-crystal optomechanical cavity”. In: *Nature* 459.7246 (2009), pp. 550–555. ISSN: 1476-4687.

[99] Matt Eichenfield et al. “Optomechanical crystals”. In: *Nature* 462.7269 (2009), p. 78. ISSN: 1476-4687.

[100] Xingwang Zhang et al. “Mode competition and hopping in optomechanical nanooscillators”. In: *Applied Physics Letters* 112.15 (2018), p. 153502.

[101] D.E. Chang et al. “Slowing and stopping light using an optomechanical crystal array”. In: *New J. Phys.* 13.2 (2011), p. 023003.

[102] M. Schmidt, M. Ludwig, and F. Marquardt. “Optomechanical circuits for nanomechanical continuous variable quantum state processing”. In: *New J. Phys.* 14.12 (2012), p. 125005.

[103] Markus Aspelmeyer, Tobias J Kippenberg, and Florian Marquardt. "Cavity optomechanics". In: *Reviews of Modern Physics* 86.4 (2014), p. 1391.

[104] Enrico Russo et al. "Optomechanical two-photon hopping". In: *Physical Review Research* 5.1 (2023), p. 013221.

[105] Federico Montalbano et al. "Spatial correlations of field observables in two half-spaces separated by a movable perfect mirror". In: *Physical Review D* 107.5 (2023), p. 056007.

[106] H. K. Cheung and C. K. Law. "Nonadiabatic optomechanical Hamiltonian of a moving dielectric membrane in a cavity". In: *Phys. Rev. A* 84 (2 2011), p. 023812.

[107] Moorad Alexanian. "Two-photon exchange between two three-level atoms in separate cavities". In: *Phys. Rev. A* 83 (2 2011), p. 023814.

[108] Y. L. Dong, S. Q. Zhu, and W. L. You. "Quantum-state transmission in a cavity array via two-photon exchange". In: *Phys. Rev. A* 85 (2 2012), p. 023833.

[109] S. Cui et al. "Nonlinear two-photon Rabi-Hubbard model: Superradiance, photon, and photon-pair Bose-Einstein condensates". In: *Phys. Rev. A* 102 (3 2020), p. 033334.

[110] A. A Stepanenko, M. D. Lyubarov, and M. A. Gorlach. "Two-photon topological States in the array of qubits caused by the effective photon-photon interaction". In: *AIP Conference Proceedings*. Vol. 2300. 1. AIP Publishing LLC. 2020, p. 020123.

[111] M. H. Nadiki and M. K. Tavassoly. "Photon blockade in a system consisting of two optomechanical cavities via photon hopping". In: *The European Physical Journal Plus* 136.3 (2021), pp. 1–12.

[112] W. Shao, C. Wu, and X.L. Feng. "Generalized James' effective Hamiltonian method". In: *Phys. Rev. A* 95 (3 2017), p. 032124.

[113] Fabrizio Minganti et al. "Dissipative state transfer and Maxwell's demon in single quantum trajectories: Excitation transfer between two noninteracting qubits via unbalanced dissipation rates". In: *Phys. Rev. A* 103 (5 2021), p. 052201.

[114] Vincenzo Macrí et al. "Revealing higher-order light and matter energy exchanges using quantum trajectories in ultrastrong coupling". In: *Physical Review A* 105.2 (2022), p. 023720.

[115] Wei Chen and Aashish A. Clerk. "Photon propagation in a one-dimensional optomechanical lattice". In: *Phys. Rev. A* 89 (3 2014), p. 033854.

[116] M. Schmidt et al. "Optomechanical creation of magnetic fields for photons on a lattice". In: *Optica* 2.7 (2015), p. 635.

[117] Jiasen Jin et al. "Photon Solid Phases in Driven Arrays of Nonlinearly Coupled Cavities". In: *Phys. Rev. Lett.* 110 (16 2013), p. 163605.

[118] William Henry Louisell. "Quantum statistical properties of radiation". In: (1973).

[119] Salvatore Savasta and Raffaello Girlanda. "The particle-photon interaction in systems described by model Hamiltonians in second quantization". In: *Solid state communications* 96.7 (1995), pp. 517–522.

[120] J. Dalibard, Y. Castin, and K. Mølmer. "Wave-function approach to dissipative processes in quantum optics". In: *Phys. Rev. Lett.* 68 (5 1992), p. 580.

[121] K. Mølmer, Yv. Castin, and J. Dalibard. "Monte Carlo wave-function method in quantum optics". In: *J. Opt. Soc. Am. B* 10.3 (1993), p. 524.

[122] H.M. Wiseman and G.J. Milburn. *Quantum Measurement and Control*. Cambridge: Cambridge University Press, 2010. ISBN: 9780521804424.

Appendix A

Hopfield-Bogoliubov transformation

A.1 Coefficients

Here we show the procedure used to obtain the explicit expression for the Hopfield coefficients. We define the polariton operator $\hat{P}_n = A_n^* \hat{a} + B_n^* \hat{b} - A_n' \hat{a}^\dagger - B_n' \hat{b}^\dagger$ that must satisfy the commutation relation:

$$\left[\hat{P}_n, \hat{\mathcal{H}}_D\right] = \Omega_n \hat{P}_n \,. \tag{A.1.1}$$

Then, we solve the resulting system for the coefficients obtained from (A.1.1) and after some algebra, we obtain the following expressions:

$$\begin{aligned} A_n =& \frac{\left|\omega_0^2 - \omega_n^2\right| \left|\omega_n^2 - \omega_c^2\right|}{2\left(\omega_n - \omega_c\right)} \times \\ & \frac{1}{\sqrt{\left(\omega_0^2 - \omega_n^2\right)^2 \omega_n \omega_c + 4\lambda^2 \omega_0 \omega_n^5}} e^{-i(\phi_n + \pi/2)} \,, \end{aligned} \tag{A.1.2}$$

$$\begin{aligned} A_n' &= \frac{\left|\omega_0^2 - \omega_n^2\right| \left|\omega_n^2 - \omega_c^2\right|}{2\left(\omega_n + \omega_c\right)} \times \\ & \frac{1}{\sqrt{\left(\omega_0^2 - \omega_n^2\right)^2 \omega_n \omega_c + 4\lambda^2 \omega_0 \omega_n^5}} e^{-i(\phi_n + \pi/2)} = \\ &= A_n \frac{\left(\omega_n - \omega_c\right)}{\left(\omega_n + \omega_c\right)} \,, \end{aligned} \tag{A.1.3}$$

$$B_n = \frac{\lambda\omega_n^2\left|\omega_0^2-\omega_n^2\right|\left|\omega_n^2-\omega_c^2\right|}{\left(\omega_n^2-\omega_c^2\right)\left(\omega_n-\omega_0\right)}\times \frac{1}{\sqrt{\left(\omega_0^2-\omega_n^2\right)^2\omega_n\omega_c+4\lambda^2\omega_0\omega_n^5}}e^{-i(\phi_n+\pi)}\,, \tag{A.1.4}$$

$$\begin{aligned} B_n' &= \frac{\lambda\omega_n^2\left|\omega_0^2-\omega_n^2\right|\left|\omega_n^2-\omega_c^2\right|}{\left(\omega_n^2-\omega_c^2\right)\left(\omega_n+\omega_0\right)}\times \frac{1}{\sqrt{\left(\omega_0^2-\omega_n^2\right)^2\omega_n\omega_c+4\lambda^2\omega_0\omega_n^5}}\,e^{i\phi_n} \\ &= B_n\frac{\left(\omega_n-\omega_0\right)}{\left(\omega_n+\omega_0\right)}e^{i(2\phi_n+\pi)}\,, \end{aligned} \tag{A.1.5}$$

The value of the phases can be obtained by imposing that $\lim_{\lambda->0}\hat{P}_n$ is either $\hat{a}$ or $\hat{b}$. For example if we choose $\omega_c<\omega_0$ we obtain that $\phi_1=\pi/2$ and $\phi_2=\pi$, and, in the $\lambda\to 0$ limit, the lower polariton $\hat{P}_1$ results the photonic operator $\hat{a}$ while $\hat{P}_2$ is the operator $\hat{b}$.

Appendix B

Minimal coupling replacement on a generic operator

By using some general operator theorems [118], we show how to implement the minimal coupling replacement on a generic operator $O(\hat{x},\hat{p})$ by a unitary transformation [119]. Given two noncommuting operators $\hat{\alpha}$ and $\hat{\beta}$ and a parameter μ we want to calculate $e^{\mu\hat{\beta}}O(\hat{\alpha})e^{-\mu\hat{\beta}}$. Let us consider the power expansion of the function $O(\hat{\alpha})$:

$$O(\hat{\alpha}) = \sum_n c_n \hat{\alpha}^n \,. \tag{B.0.1}$$

It follows that

$$e^{\mu\hat{\beta}}O(\hat{\alpha})e^{-\mu\hat{\beta}} = \sum_n c_n e^{\mu\hat{\beta}}\hat{\alpha}^n e^{-\mu\hat{\beta}} \,. \tag{B.0.2}$$

Observing that

$$e^{\mu\hat{\beta}}\hat{\alpha}^n e^{-\mu\hat{\beta}} = e^{\mu\hat{\beta}}\hat{\alpha}e^{-\mu\hat{\beta}}e^{\mu\hat{\beta}}\hat{\alpha}e^{-\mu\hat{\beta}}\ldots e^{\mu\hat{\beta}}\hat{\alpha}e^{-\mu\hat{\beta}} = \left(e^{\mu\hat{\beta}}\hat{\alpha}e^{-\mu\hat{\beta}}\right)^n \,. \tag{B.0.3}$$

We have:

$$e^{\mu\hat{\beta}}O(\hat{\alpha})e^{-\mu\hat{\beta}} = \sum_n c_n \left(e^{\mu\hat{\beta}}\hat{\alpha}e^{-\mu\hat{\beta}}\right)^n = O(e^{\mu\hat{\beta}}\hat{\alpha}e^{-\mu\hat{\beta}}) \,. \tag{B.0.4}$$

We now apply (B.0.4) to $e^{i\chi(\hat{x})/\hbar}O(\hat{x},\hat{p})e^{-i\chi(\hat{x})/\hbar}$. For simplicity's sake, we consider the 1D case. The generalisation to 3D is straightforward. We obtain

$$e^{i\hat{\chi}(x)/\hbar}O(x,\hat{p})e^{-i\hat{\chi}(x)/\hbar} = O(x, e^{i\hat{\chi}(x)/\hbar}\hat{p}e^{-i\chi(x)/\hbar}) \,. \tag{B.0.5}$$

Then we use the Baker-Campbell-Hausdorff Lemma:

$$\begin{aligned} e^{i\hat{\chi}(x)/\hbar}\hat{p}e^{-i\hat{\chi}(x)/\hbar} &= \hat{p} + \frac{i}{\hbar}\left[\hat{\chi}(x),\hat{p}\right] + \frac{1}{2}\left(\frac{i}{\hbar}\right)^2\left[\chi(\hat{x}),\left[\chi(\hat{x}),\hat{p}\right]\right] + \ldots \\ &= \hat{p} - \partial_x\hat{\chi}(x) \end{aligned} \tag{B.0.6}$$

where we have used the result $[\hat{\chi}(x), \hat{p}] = i\hbar\partial_x\hat{\chi}(x)$. In conclusion, using (B.0.6), (B.0.5) becomes

$$e^{i\hat{\chi}(x)/\hbar}O(x,\hat{p})e^{-i\hat{\chi}(x)/\hbar} = O(x, \hat{p} - \partial_x\hat{\chi}(x))\,. \tag{B.0.7}$$

Let us introduce the special function

$$\hat{\chi}(x) = x\hat{A}_0\,, \tag{B.0.8}$$

where $\hat{A}_0 \equiv \hat{A}(x_0)$ is the field potential calculated at the atom position x_0, we obtain

$$\partial_x\hat{\chi}(x) = \hat{A}_0\,. \tag{B.0.9}$$

Thus, Eq. (B.0.7) becomes:

$$e^{i\hat{\chi}(x)/\hbar}O(x,\hat{p})e^{-i\hat{\chi}(x)/\hbar} = O(x, \hat{p} - \hat{A}_0)\,, \tag{B.0.10}$$

demonstrating that the unitary transformation in Eq. (B.0.7) corresponds to the application of the minimal coupling replacement in the dipole approximation.

Appendix C

Analytical derivation of the pure dephasing rates

We consider the Coulomb gauge and using eq. (3.1.6), we discard the off-diagonal terms Γ_{ϕ}^{jk} since this contribution is significant only if the dephasing bath has a spectral weight at the potentially high frequency ω_{jk}, leading to the following equation:

$$\dot{\hat{\rho}} = -i\Big[\hat{\mathcal{H}}_C, \hat{\rho}\Big] + \frac{\gamma_\phi(0)}{2}\mathcal{D}\left[\sum_j \sigma_z^{C,jj} \left|j\right\rangle\!\left\langle j\right|\right]\hat{\rho}\,, \tag{C.0.1}$$

where $\sigma_z^{C,jj} = \langle j|\hat{\sigma}_z|j\rangle$. We now expand the Lindblad dissipator

$$\begin{aligned}\mathcal{D}\left[\sum_j \sigma_z^{C,jj} \left|j\right\rangle\!\left\langle j\right|\right]\hat{\rho} =& \frac{1}{2}\left[2\sum_j\sum_{j'}\sigma_z^{C,jj}\sigma_z^{C,j'j'}\left|j\right\rangle\!\left\langle j\right|\hat{\rho}\left|j'\right\rangle\!\left\langle j'\right| + \right.\\ &- \sum_j\sum_{j'}\sigma_z^{C,jj}\sigma_z^{C,j'j'}\left|j'\right\rangle\left\langle j'|j\right\rangle\left\langle j\right|\hat{\rho}\\ &\left.- \sum_j\sum_{j'}\sigma_z^{C,jj}\sigma_z^{C,j'j'}\hat{\rho}\left|j'\right\rangle\left\langle j'|j\right\rangle\left\langle j\right|\right],\end{aligned} \tag{C.0.2}$$

and we focus on the matrix element of the density matrix relative to the transition $(\tilde{1}_-, \tilde{0})$, but the same procedure can be applied to all the other transitions. The corre-

sponding equation (in the interaction picture) for that matrix element becomes

$$\begin{aligned}
\frac{d}{dt}\hat{\rho}^{(I)}_{\tilde{1}_-,\tilde{0}} &= \frac{\gamma_\phi(0)}{4}\langle\tilde{1}_-|\left[2\sum_j\sum_{j'}\sigma_z^{C,jj}\sigma_z^{C,j'j'}|j\rangle\langle j|\hat{\rho}^{(I)}|j'\rangle\langle j'| + \right. \\
&\qquad \left. -\sum_j|\sigma_z^{C,jj}|^2|j\rangle\langle j|\hat{\rho}^{(I)} - \sum_j|\sigma_z^{C,jj}|^2\hat{\rho}^{(I)}|j\rangle\langle j|\right]|\tilde{0}\rangle \\
&= \frac{\gamma_\phi(0)}{4}\left[2\sum_j\sum_{j'}\sigma_z^{C,jj}\sigma_z^{C,j'j'}\langle\tilde{1}_-|j\rangle\langle j|\hat{\rho}^{(I)}|j'\rangle\langle j'|\tilde{0}\rangle + \right. \\
&\qquad \left. -\sum_j|\sigma_z^{C,jj}|^2\langle\tilde{1}_-|j\rangle\langle j|\hat{\rho}^{(I)}|\tilde{0}\rangle\sum_j|\sigma_z^{C,jj}|^2\langle\tilde{1}_-|\hat{\rho}^{(I)}|j\rangle\langle j|\tilde{0}\rangle\right] \\
&= \frac{\gamma_\phi(0)}{4}\left[2\sigma_z^{C,\tilde{1}_-\tilde{1}_-}\sigma_z^{C,\tilde{0}\tilde{0}}\langle\tilde{1}_-|\hat{\rho}^{(I)}|\tilde{0}\rangle + \right. \\
&\qquad \left. -|\sigma_z^{C,\tilde{1}_-\tilde{1}_-}|^2\langle\tilde{1}_-|\hat{\rho}^{(I)}|\tilde{0}\rangle - |\sigma_z^{C,\tilde{0}\tilde{0}}|^2\langle\tilde{1}_-|\hat{\rho}^{(I)}|\tilde{0}\rangle\right] \\
&= -\frac{\gamma_\phi(0)}{4}\left|\sigma_z^{C,\tilde{1}_-\tilde{1}_-} - \sigma_z^{C,\tilde{0}\tilde{0}}\right|^2\hat{\rho}^{(I)}_{\tilde{1}_-,\tilde{0}}\,.
\end{aligned} \tag{C.0.3}$$

By choosing the dipole gauge, one should replace $\sigma_z^{C,jj} \to \sigma_z^{jj}$. The same procedure is valid also for cavity pre dephasing, where we need to use $\hat{a}^\dagger\hat{a}$ in the Coulomb gauge and $\hat{a}_D^\dagger\hat{a}_D$ in the dipole gauge.

Appendix D

Optomechanics

D.1 Derivation of the classical optomechanical Hamiltonian

Our starting point is two non-interacting electromagnetic cavities, with a movable perfect mirror separating them. We follow the methodology outlined in Ref. [79] and, in order to simplify the process, we conduct our analysis in one dimension and then we generalize our findings to our specific case. In terms of notation, we use $\pm I$ to refer to the endpoints of the cavity, while M and $q(t)$ denote the mass and position of the movable mirror, respectively. Since there are no charges present, the electromagnetic field follows the wave equation. However, the motion of the movable mirror is impacted by the radiation pressure of the fields in both cavities, as depicted in Fig. 2(a) in the main text. Therefore, it follows the laws of motion as outlined by Newton's equation.

$$\begin{cases} \Delta A = 0 & x \in (-I, q) \cup (q, I) \\ M\ddot{q} = -\partial_q V + \frac{1}{2}\left[(\partial_- A)^2 - (\partial_+ A)^2\right]|_q \end{cases} \tag{D.1.1}$$

where $\Delta := \partial_t^2 - \partial_x^2$ and ∂_-, ∂_+ are the left and right derivatives. We consider the potential $V(q)$ to be infinite at the two mirror positions $\pm I$. Considering a movable mirror of negligible thickness, the two radiation pressures $(\partial_\pm A)^2/2$ come with opposite signs and in the form of lateral derivatives.

By defining L_k and R_k as the Fourier components on the left and right cavity, respectively, the completeness of the mode functions enables to write (from now on, we adopt

the Einstein summation convention),

$$A(t,x) = \begin{cases} L^k(t)\,\varphi_k(t,x) & x \in (-I, q) \\ R^k(t)\,\phi_k(t,x) & x \in (q, I) \end{cases} \tag{D.1.2}$$

where the summation in k is understood and,

$$\begin{aligned} \varphi_k &= \sqrt{\frac{2}{q+I}} \sin\left[\omega_k(x+I)\right] , \\ \phi_k &= \sqrt{\frac{2}{I-q}} \sin\left[\Omega_k(x-I)\right] , \end{aligned} \tag{D.1.3}$$

with $\omega_k = k\pi/(q+I)$, $\Omega_k = k\pi/(I-q)$. We can still fix a normalisation for φ_k and ϕ_k choosing,

$$\delta_{ij} = \int_{-I}^{q} \varphi_i \varphi_j = \int_{q}^{I} \phi_i \phi_j , \tag{D.1.4}$$

as the Kronecker delta. The wave equation (D.1.1) can be projected along one Fourier component, and the equation of motion of the movable mirror becomes,

$$\begin{aligned} \ddot{L}_k + \omega_k^2 L_k - \frac{g_{km}\left(2\dot{q}\dot{L}^m + \ddot{q}L^m\right)}{I+q} + \dot{q}^2 \frac{\left(g_{km} + g_{kj}g^j{}_m\right) L^m}{(I+q)^2} &= 0 , \\ \ddot{R}_k + \Omega_k^2 R_k - \frac{\gamma_{km}\left(2\dot{q}\dot{R}^m + \ddot{q}R^m\right)}{I-q} - \dot{q}^2 \frac{\left(\gamma_{km} - \gamma_{kj}\gamma^j{}_m\right) R^m}{(I-q)^2} &= 0 , \\ M\ddot{q} + \partial_q V + (-1)^{k+m}\left(\frac{\Omega_k\Omega_m R^k R^m}{I-q} - \frac{\omega_k\omega_m L^k L^m}{q+I}\right) &= 0 , \end{aligned} \tag{D.1.5}$$

with,

$$g_{km} = (q+I)\int_{-I}^{q} \partial_q(\varphi_k)\varphi_m = -\gamma_{km} = -(I-q)\int_{q}^{I} \partial_q(\phi_k)\phi_m , \tag{D.1.6}$$

that satisfy,

$$g_{kj}g^j{}_m = -(q+I)^2 \int_{-I}^{q} \partial_q\varphi_k \partial_q\varphi_m = \gamma_{kj}\gamma^j{}_m = -(I-q)^2 \int_{q}^{I} \partial_q\phi_k \partial_q\phi_m , \tag{D.1.7}$$

and

$$\begin{aligned} \int_{-I}^{q} \varphi_k \partial_q^2 \varphi_m &= \frac{1}{(q+I)^2}\left(g_{kj}g^j{}_m - g_{km}\right) , \\ \int_{q}^{I} \phi_k \partial_q^2 \phi_m &= \frac{1}{(I-q)^2}\left(\gamma_{kj}\gamma^j{}_m + \gamma_{km}\right) . \end{aligned} \tag{D.1.8}$$

The system of equations (D.1.1) can be derived from the following Lagrangian,

$$\begin{aligned}\mathcal{L}(q,\dot{q},L,\dot{L},R,\dot{R}) =& \frac{1}{2}\left(\dot{L}_k\dot{L}^k - \omega_k^2 L_k L^k + \dot{R}_k\dot{R}^k - \Omega_k^2 R_k R^k\right) + \\ &- \dot{q}\left(g_{km}\frac{\dot{L}^k L^m}{q+I} + \gamma_{km}\frac{\dot{R}^k R^m}{I-q}\right) + \\ &- \frac{\dot{q}^2}{2}\left[g_{kj}g^j{}_m\frac{L^k L^m}{(q+I)^2} + \gamma_{kj}\gamma^j{}_m\frac{R^k R^m}{(I-q)^2}\right] + \frac{1}{2}M\dot{q}^2 - V\,,\end{aligned} \tag{D.1.9}$$

and the corresponding Hamiltonian is,

$$\begin{aligned}\mathcal{H}(q,p,L,\Lambda,R,W) =& \frac{1}{2M}\left(p + g_{km}\frac{\Lambda^k L^m}{q+I} + \gamma_{km}\frac{W^k R^m}{I-q}\right)^2 + \\ &+ V + \frac{1}{2}\left(\Lambda_k\Lambda^k + \omega_k^2 L^k L^k\right) + \frac{1}{2}\left(W_k W^k + \Omega_k^2 R^k R^k\right)\,.\end{aligned} \tag{D.1.10}$$

Let us first examine the classical system equations presented in (D.1.5) before quantizing the classical Hamiltonian as shown in (D.1.10). The equations that govern L_k and R_k are homogeneous, and their coefficients are non-trivial functions of q, $\dot{q}$, and $\ddot{q}$. If the initial condition is given as $R_k(0) = \dot{R}_k(0) = 0$, which implies that there is no field present on the right side of the cavity at the starting time, then the solution $R_k(t) = 0$ holds true for all times. This is a well-posed Cauchy problem, and as such, the solution of the equation is unique. Therefore, regardless of what values L_k may take, $R_k(t)$ will remain zero. Furthermore, if we consider the energy of the right electromagnetic field,

$$\begin{aligned}\mathcal{U} &= \frac{1}{2}\int_q^I [(\dot{A})^2 + (\partial_x A)^2]dx \\ &= \frac{1}{2}[\dot{R}^k\dot{R}_k - \frac{\dot{q}^2}{(I-q)^2}\gamma_{ki}\gamma^i_j R^k R^j]\,,\end{aligned} \tag{D.1.11}$$

by virtue of (D.1.2), (D.1.3), (D.1.4) and (D.1.7) (the sum over k, i and j is understood). The energy present in the system is evidently linked to the states of the mechanical mirrors, dictated by the equations of motion. If the right cavity does not contain any photons, it follows that the energy in the system will remain at zero, which in turn prevents the left electromagnetic field from being transferred to the right side. These properties of the system reflect the perfection of the mirrors and the fact that the classical vacuum is empty.

D.2 Quantization of the classical system Hamiltonian

Consider the operators $\{\hat{q}, \hat{p}, \hat{L}_k, \hat{\Lambda}_k, \hat{R}_k, \hat{W}_k\}$ and impose the commutation relations ($\hbar = 1$), $[\hat{q}, \hat{p}] = i$, $[\hat{L}_k, \hat{\Lambda}_m] = i\delta_{km}$ and $[\hat{R}_k, \hat{W}_m] = i\delta_{km}$, while $[\hat{q}, \hat{L}_m] = [\hat{q}, \hat{R}_m] = [\hat{L}_k, \hat{R}_m] = [\hat{p}, \hat{L}_m] = [\hat{p}, \hat{W}_m] = [\hat{\Lambda}_k, \hat{W}_m] = 0$. Using the ladder operators,

$$\begin{aligned} \hat{a}_k &= \frac{1}{\sqrt{2\omega_k}} \left(\omega_k \hat{L}_k + i\hat{\Lambda}_k\right) , \\ \hat{c}_k &= \frac{1}{\sqrt{2\Omega_k}} \left(\Omega_k \hat{R}_k + i\hat{W}_k\right) , \end{aligned} \tag{D.2.1}$$

the Hamiltonian (D.1.10) becomes,

$$\begin{aligned} \hat{H}' =& \frac{(\hat{p} + \hat{\Gamma})^2}{2M} + \hat{V} + \sum_k \omega_k \hat{a}_k^\dagger \hat{a}_k \\ &+ \sum_k \Omega_k \hat{c}_k^\dagger \hat{c}_k - \frac{\pi q \hat{\mathbb{1}}}{6(q+I)(q-I)} , \end{aligned} \tag{D.2.2}$$

where we have already resummed the vacuum point fluctuations, and

$$\begin{aligned} \hat{\Gamma} = \frac{i}{2}\sqrt{\frac{m}{k}} \Bigg[& \frac{g^{km}(\hat{a}_k^\dagger - \hat{a}_k)(\hat{a}_m^\dagger + \hat{a}_m)}{q+I} \\ & + \frac{\gamma^{km}(\hat{c}_k^\dagger - \hat{c}_k)(\hat{c}_m^\dagger + \hat{c}_m)}{I-q} \Bigg] . \end{aligned} \tag{D.2.3}$$

This is the full Hamiltonian of the problem. Eq. (1) in the main text is obtained by considering the unimodal case and linearising it. To do this we first consider $\Gamma \approx \Gamma_0$ constant and then introduce a variation from the expected position of the mirror $q = q_0 + \delta q$, and expand all the terms accordingly,

$$\begin{aligned} \omega_k &= \frac{k\pi}{q_0 + I}\left(1 - \frac{\delta q}{q_0 + I}\right) + \mathcal{O}\left[\frac{\delta q^2}{(q_0+I)^2}\right] , \\ \Omega_k &= \frac{k\pi}{I - q_0}\left(1 + \frac{\delta q}{I - q_0}\right) + \mathcal{O}\left[\frac{\delta q^2}{(I-q_0)^2}\right] , \end{aligned} \tag{D.2.4}$$

which in turn, from (D.2.1), induces

$$\begin{aligned} \hat{a}_k &\approx (\hat{a}_0)_k - \frac{\delta q}{2(q_0+I)}(\hat{a}_0^\dagger)_k , \\ \hat{c}_k &\approx (\hat{c}_0)_k + \frac{\delta q}{2(I-q_0)}(\hat{c}_0^\dagger)_k . \end{aligned} \tag{D.2.5}$$

Performing the unitary transformation $\hat{U} = \exp(i\delta q \hat{\Gamma}_0)$ on (D.2.2), proves that,

$$\begin{aligned} \hat{H} = \hat{U}\hat{H}'\hat{U}^\dagger = \frac{\hat{p}^2}{2M} + \hat{\mathcal{V}} + \sum_k \Big[& (\omega_0)_k (\hat{a}_0^\dagger)_k (\hat{a}_0)_k \\ & + (\Omega_0)_k (\hat{c}_0^\dagger)_k (\hat{c}_0)_k \Big] - \delta q (\hat{G}_0 + \hat{F}_0) , \end{aligned} \tag{D.2.6}$$

where $\hat{\mathcal{V}} = \hat{V} - \pi q \hat{\mathbb{1}}/6(q+I)(q-I)$, and

$$\hat{F}_0 = \sum_{k,j} \frac{(-1)^{k+j}}{2(q_0+I)} \sqrt{(\omega_k \omega_j)_0}\, (\hat{a}_k^\dagger + \hat{a}_k)(\hat{a}_j^\dagger + \hat{a}_j)\,,$$
$$\hat{G}_0 = \sum_{k,j} \frac{(-1)^{k+j+1}}{2(I-q_0)} \sqrt{(\Omega_k \Omega_j)_0}\, (\hat{c}_k^\dagger + \hat{c}_k)(\hat{c}_j^\dagger + \hat{c}_j)\,. \tag{D.2.7}$$

Finally, we consider a quadratic potential V and introduce the vibrating mirror ladder operators $\{b, b^\dagger\}$ in a way that $\delta q = x_{\rm zpf}(b + b^\dagger)$, where $x_{\rm zpf}$ is the zero-point-fluctuation amplitude of the vibrating mirror. By reducing all the modes to one ($k = j = 1$), the system Hamiltonian in (D.2.2) can be written down as,

$$\hat{H} = \omega_a \hat{a}^\dagger \hat{a} + \omega_b \hat{b}^\dagger \hat{b} + \omega_c \hat{c}^\dagger \hat{c}$$
$$+ \frac{x_{\rm zpf}}{2\pi} \left[\omega_c^2 (\hat{c} + \hat{c}^\dagger)^2 - \omega_a^2 (\hat{a} + \hat{a}^\dagger)^2\right] (\hat{b} + \hat{b}^\dagger)\,. \tag{D.2.8}$$

Defining a coupling strength $g = \omega_c^2\, x_{\rm zpf}/\pi = \omega_c\, x_{\rm zpf}/(I - q_0)$ the (4.2.1) in the main text is obtained. Note that since $\hbar = 1$ the coupling strength g has the right units.

D.3 Effective Hamiltonian with the generalized James' method

The generalized James' effective Hamiltonian method [112] allows us to obtain an effective Hamiltonian for strongly detuned quantum systems. To apply this method to (4.2.1) in the main text, we first rewrite it in the interaction picture,

$$\hat{H}_{\rm I}(t) = g \left[\hat{c}^\dagger \hat{c} - \frac{\omega_a^2}{\omega_c^2} \hat{a}^\dagger \hat{a}\right] \hat{b}\, e^{-i\omega_b t} + \frac{g}{2} \left[(\hat{c})^2 \hat{b}\, e^{-i(\omega_b + 2\omega_c)t} - \frac{\omega_a^2}{\omega_c^2} (\hat{a})^2 \hat{b}\, e^{-i(\omega_b + 2\omega_a)t}\right]$$
$$+ \frac{g}{2} \left[(\hat{c}^\dagger)^2 \hat{b}\, e^{i(2\omega_c - \omega_b)t} - \frac{\omega_a^2}{\omega_c^2} (\hat{a}^\dagger)^2 \hat{b}\, e^{i(2\omega_a - \omega_b)t}\right] + \text{h.c.}\,. \tag{D.3.1}$$

This can be rewritten as,

$$\hat{H}_{\rm I}(t) = \sum_k \left[\hat{h}_k e^{-i\omega_k t} + \hat{h}_k^\dagger e^{i\omega_k t}\right]\,, \tag{D.3.2}$$

where now the ω_k are a combination of the bare transition frequencies. The second-order generalized James' effective Hamiltonian already shows a photon-pair hopping mechanism. The second order effective Hamiltonian is:

$$\hat{H}_{\rm I}^{(2)}(t) = \sum_{j,k} \frac{1}{\omega_k} \left[\hat{h}_j \hat{h}_k^\dagger e^{i(\omega_k - \omega_j)t} - \hat{h}_j^\dagger \hat{h}_k e^{i(\omega_j - \omega_k)t}\right]\,. \tag{D.3.3}$$

We can neglect all frequency contributions which are different from zero by applying the rotating-wave approximation. Since the frequencies ω_k are all different, we only keep the terms in $\hat{H}_{\mathrm{I}}^{(2)}(t)$ where the sum of the exponent is zero.

Starting from (D.3.1) and considering the resonant condition $\omega_a = \omega_c$, only three terms need to be considered,

$$\begin{aligned} \hat{h}_1 &= \frac{g}{2}(\hat{c}^{\dagger 2} - \hat{a}^{\dagger 2})\hat{b}^\dagger && \omega_1 = 2\omega_a + \omega_b, \\ \hat{h}_2 &= \frac{g}{2}(\hat{c}^{\dagger 2} - \hat{a}^{\dagger 2})\hat{b} && \omega_2 = 2\omega_a - \omega_b, \\ \hat{h}_3 &= \frac{g}{2}\left(\{\hat{c}, \hat{c}^\dagger\} - \{\hat{a}, \hat{a}^\dagger\}\right)\hat{b}^\dagger && \omega_3 = \omega_b\,. \end{aligned} \tag{D.3.4}$$

From the canonical commutation relations it follows that,

$$\begin{aligned} \left[\hat{h}_1, \hat{h}_1^\dagger\right] =& \frac{g^2}{4}\left[\hat{a}^2\hat{c}^{\dagger 2} + \hat{a}^{\dagger 2}\hat{c}^2 - \hat{c}^{\dagger 2}\hat{c}^2 - \hat{a}^{\dagger 2}\hat{a}^2 + 2\hat{b}^\dagger\hat{b}\left(\{\hat{c}, \hat{c}^\dagger\} + \{\hat{a}, \hat{a}^\dagger\}\right)\right], \\ \left[\hat{h}_2, \hat{h}_2^\dagger\right] =& \frac{g^2}{4}\left[\hat{c}^{\dagger 2}\hat{c}^2 + \hat{a}^{\dagger 2}\hat{a}^2 - \hat{c}^{\dagger 2}\hat{a}^2 - \hat{a}^{\dagger 2}\hat{c}^2 + 2\hat{b}\hat{b}^\dagger\left(\{\hat{c}, \hat{c}^\dagger\} + \{\hat{a}, \hat{a}^\dagger\}\right)\right], \\ \left[\hat{h}_3, \hat{h}_3^\dagger\right] =& -g^2(\hat{c}^\dagger\hat{c} - \hat{a}^\dagger\hat{a})^2\,, \end{aligned} \tag{D.3.5}$$

so James' effective Hamiltonian is,

$$\begin{aligned} \hat{H}_{\mathrm{eff}}^{(2)} =& \left[\omega_a + \frac{g^2(4\omega_a + \omega_b)}{8\omega_a^2 - 2\omega_b^2}\right](\hat{c}^\dagger\hat{c} + \hat{a}^\dagger\hat{a}) + \qquad (\text{D.3.6}) \\ &+ \frac{g^2(3\omega_b^2 - 8\omega_a^2)}{(8\omega_a^2 - 2\omega_b^2)\omega_b}[(\hat{c}^\dagger\hat{c})^2 + (\hat{a}^\dagger\hat{a})^2] + \frac{2g^2}{\omega_b}\hat{a}^\dagger\hat{a}\hat{c}^\dagger\hat{c} + \frac{g^2\hat{\mathbb{1}}}{2\omega_a - \omega_b} + \\ &+ \left[\omega_b + \frac{4g^2\omega_a}{4\omega_a^2 - \omega_b^2}(\hat{c}^\dagger\hat{c} + \hat{a}^\dagger\hat{a} + \hat{\mathbb{1}})\right]\hat{b}^\dagger\hat{b} - \frac{g^2\omega_b}{8\omega_a^2 - 2\omega_b^2}(\hat{a}^2\hat{c}^{\dagger 2} + \hat{a}^{\dagger 2}\hat{c}^2)\,. \qquad (\text{D.3.7}) \end{aligned}$$

All the terms but the last one are energy shifts. The latter is the desired hopping mechanism.

D.4 Monte Carlo wave function approach: Quantum trajectory

The Monte Carlo wave function (MCWF) approach is introduced in Refs. [120, 121] by describing the effect of the environment between two quantum jumps through a non-Hermitian Hamiltonian:

$$\hat{\mathcal{H}} = \hat{H} - \frac{i}{2}\sum_m \gamma_m \hat{\Gamma}_m^\dagger\hat{\Gamma}_m\,. \tag{D.4.1}$$

Here, $\hat{H}$ represents the Hamiltonian part of the dynamics, either the full one or obtained through approximation methods, and $\hat{\Gamma}_m$ are the jump operators. The evolution of a quantum trajectory is thus dictated by a non-Hermitian evolution via $\hat{\mathcal{H}}$ interrupted by random quantum jumps. The algorithm to obtain such a dynamics reads:

(i) $|\psi(t)\rangle$ is the normalized wave function at the initial time t.

(ii) The probability that a quantum jump occurs through the m-th dissipative channel in a small amount of time dt is,

$$\delta p_m(t) = dt\gamma_m \langle\psi(t)|\hat{\Gamma}_m^\dagger \hat{\Gamma}_m|\psi(t)\rangle \ , \tag{D.4.2}$$

such that $\delta p_m(t) \ll 1$.

(iii) One randomly generates a real number $\varepsilon \in [0,1]$.

(iv) If $\sum_m \delta p_m(t) < \varepsilon$, no quantum jump occurs, and the system evolves as,

$$|\psi(t+dt)\rangle = \exp\left(-i\hat{\mathcal{H}}dt\right) = \mathbb{1} - idt\hat{\mathcal{H}}\,|\psi(t)\rangle + \mathcal{O}(dt^2)\,. \tag{D.4.3}$$

(v) Otherwise, if $\sum_m \delta p_m(t) > \varepsilon$, a quantum jump occurs. To decide which channel dissipates, a second random number ε' is generated, and each quantum jump is selected with probability $\delta p_m(t)/(\sum_n \delta p_n(t))$. The wave function then becomes,

$$|\psi(t+dt)\rangle = \hat{\Gamma}_m\,|\psi(t)\rangle \ . \tag{D.4.4}$$

(vi) At this point, independently of whether a quantum jump took place, the wave function $|\psi(t+dt)\rangle$ is renormalized and used for the next step of the time evolution.

A quantum jump corresponds to the projection of the wave function associated with a generalized measurement process (wave-function collapse through a positive operator-valued measure) [122].

Averaging over an infinite number of trajectories allows us the certainty to obtain the Lindblad master equation results. Concretely, the number of trajectories needed to obtain the convergence of the two approaches is determined by noise effects.